


FULL PAPER

Open Access



# Surface rupture and characteristics of a fault associated with the 2011 and 2016 earthquakes in the southern Abukuma Mountains, northeastern Japan, triggered by the Tohoku-Oki earthquake

Keitaro Komura<sup>1,2\*</sup> , Kotaro Aiyama<sup>1</sup>, Takahiro Nagata<sup>3</sup>, Hiroshi P. Sato<sup>4</sup>, Akihiro Yamada<sup>5</sup> and Yasuhira Aoyagi<sup>1</sup>

## Abstract

The 2011 Tohoku-Oki offshore subduction earthquake ( $M_w$  9.0) triggered many normal-type earthquakes inland in northeastern Japan. Among these were two very similar normal-faulting earthquakes in 2011 ( $M_w$  5.8) and 2016 ( $M_w$  5.9), which created surface ruptures along the newly named Mochiyama fault within the southern Abukuma Mountains, northeastern Japan, where no active faults had been previously mapped by interpretation of aerial photographs. We conducted field surveys in this area immediately after both earthquakes, and we performed trench excavations and observations of fault fracture zones after the 2016 event. These activities were complemented by an interferometric synthetic aperture radar analysis that mapped the areas of deformation and locations of surface discontinuities for both events. The combined results document the coseismic behavior of the Mochiyama fault during both events. Subtle tectonic geomorphic features associated with the fault were evident in a lidar digital elevation model of the area, and layered structures of gouge were documented in the field. These lines of evidence indicate repeated activity at shallow crustal levels and the possibility of Quaternary activity. In addition, our trench excavations revealed at least one faulting event before 2011. Our comparison of paleoseismic records on this and two other normal faults in the Abukuma Mountains suggests that great earthquakes in the Japan Trench supercycle of 500–700 years do not consistently trigger ruptures on these faults, and the case of 2011, in which the Tohoku-Oki megathrust earthquake triggered all three faults, is a rare occurrence.

**Keywords:** Normal fault, Surface rupture, Fault fracture zone, InSAR, Lidar DEM, Trench excavation, Paleoseismology, 2011 Tohoku-Oki earthquake, 2011 Iwaki earthquake, The Abukuma Mountains

## Introduction

The 2011 Tohoku-Oki subduction earthquake ( $M_w$  9.0) triggered many normal-type earthquakes in northeastern Japan, in the hanging wall of the convergent plate boundary along the Japan Trench (e.g., Kato et al. 2011; Okada et al. 2011; Imanishi et al. 2012). The southern Abukuma Mountains, an area ~240 km southwest of the

Tohoku-Oki epicenter measuring ~170 km from north to south and ~50 km from east to west, experienced many shallow normal-type earthquakes. The largest of these, the 11 April 2011 Iwaki earthquake ( $M_w$  6.6), produced two subparallel surface ruptures ~15-km long and 14-km long (Fig. 1; Mizoguchi et al. 2012; Toda and Tsutsumi 2013).

Two other triggered earthquakes, a  $M_w$  5.8 event on 19 March 2011 and a  $M_w$  5.9 event on 28 December 2016, struck the same part of the southern Abukuma Mountains (Fig. 1). Surface displacements associated with both earthquakes were detected by differential interferometric

\*Correspondence: komukeit@criepi.denken.or.jp

<sup>1</sup> Central Research Institute of Electric Power Industry, 1646 Abiko, Abiko-shi, Chiba 270-1194, Japan

Full list of author information is available at the end of the article

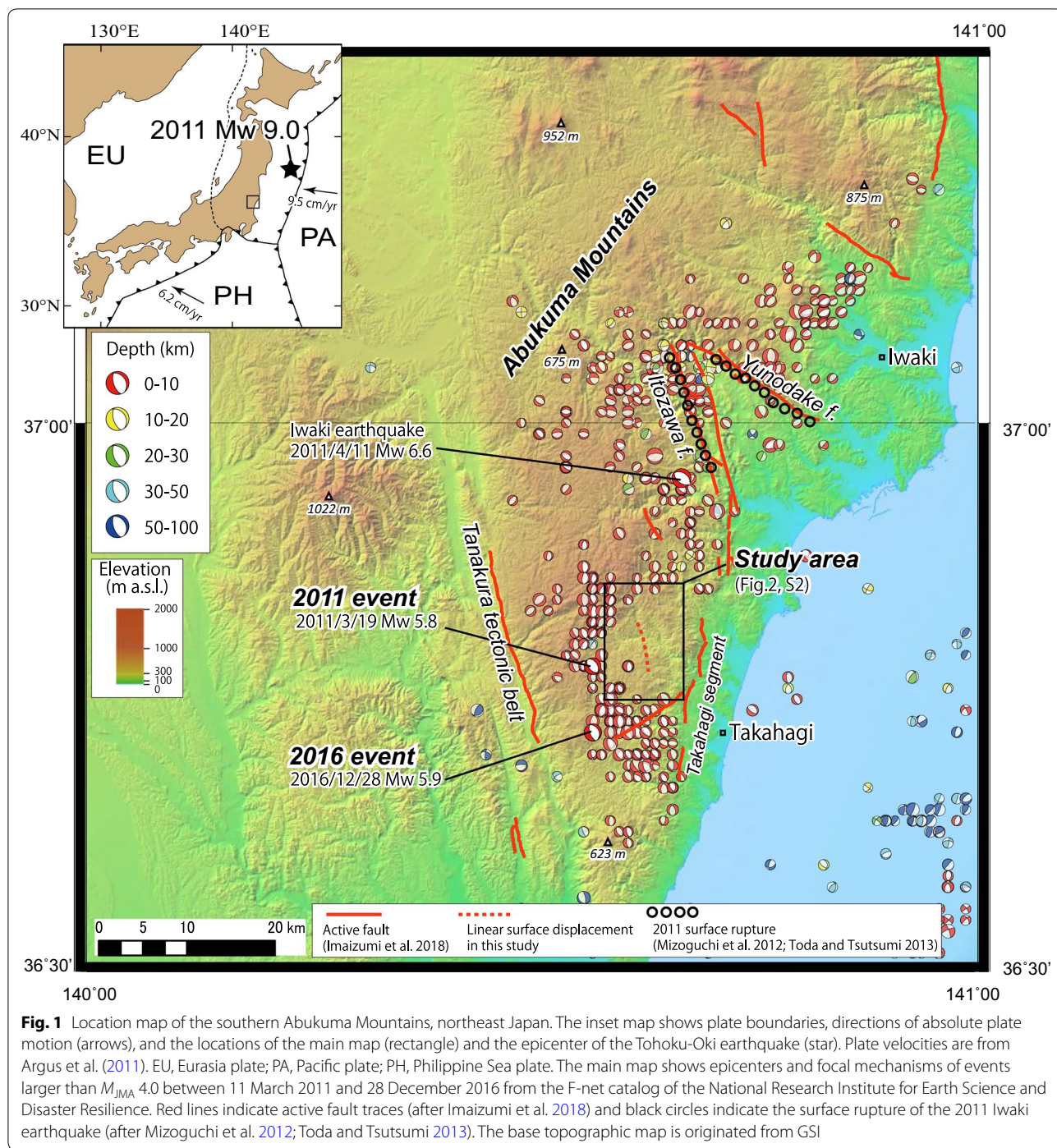


**Fig. 1** Location map of the southern Abukuma Mountains, northeast Japan. The inset map shows plate boundaries, directions of absolute plate motion (arrows), and the locations of the main map (rectangle) and the epicenter of the Tohoku-Oki earthquake (star). Plate velocities are from Argus et al. (2011). EU, Eurasia plate; PA, Pacific plate; PH, Philippine Sea plate. The main map shows epicenters and focal mechanisms of events larger than  $M_{JMA}$  4.0 between 11 March 2011 and 28 December 2016 from the F-net catalog of the National Research Institute for Earth Science and Disaster Resilience. Red lines indicate active fault traces (after Imaizumi et al. 2018) and black circles indicate the surface rupture of the 2011 Iwaki earthquake (after Mizoguchi et al. 2012; Toda and Tsutsumi 2013). The base topographic map is originated from GSI

synthetic aperture radar (InSAR) studies (Kobayashi et al. 2011; Fukushima et al. 2018). Fukushima et al. (2018) reported that both earthquakes involved slip on the same fault plane and proposed that the large postseismic crustal deformation of the Tohoku-Oki earthquake promoted the extremely short recurrence interval represented by these events. However, no detailed field survey has been

reported for either event. Detailed field observations and paleoseismic studies related to these events are required to evaluate the probabilities of triggered earthquake activity associated with megathrust earthquakes.

InSAR images obtained from observations before and after recent inland earthquakes have revealed ground displacements as small as a few centimeters (e.g., Wei et al.

2011; Fujiwara et al. 2016, 2019; Ponti et al. 2019; Choi et al. 2019), although whether these displacements were due to tectonic or non-tectonic causes is unclear. InSAR is useful for mapping surface ruptures, and comparisons of short-term ground displacements in an InSAR analysis and tectonic features visible in high-resolution lidar digital elevation models (DEMs) and paleoseismic investigations have led to better understanding of long-term fault behavior.

After the 2011 and 2016 earthquakes, we immediately conducted field surveys and revealed surface ruptures and fault fracture zones (FFZs) that define a single active fault, which we name the Mochiyama fault. In this paper, the combined results of field observations, InSAR analysis, and DEM interpretation revealed the behavior and repetitive activity of the Mochiyama fault and relationship with paleoearthquakes on other faults in the southern Abukuma Mountains and the supercycle of megathrust earthquakes along the Japan Trench.

### Tectonic setting

The Abukuma Mountains are in the southeastern part of northern Honshu Island, on the hanging wall of the convergent plate boundary along the Japan Trench and southwest of the epicenter of the 2011 Tohoku-Oki earthquake (inset of Fig. 1). Much of northern Honshu had been considered to be under an E–W compressional stress field before the Tohoku-Oki earthquake (e.g., Suwa et al. 2006; Meneses-Gutierrez and Sagiya 2016), but in the southern Abukuma Mountains, the stress field abruptly changed to extensional stress after the earthquake (e.g., Kato et al. 2011; Okada et al. 2011; Toda et al. 2011). However, some studies have suggested that the southern Abukuma Mountains had an extensional stress field before the Tohoku-Oki earthquake (Imanishi et al. 2012; Otsubo et al. 2018), and two or three active normal faults have been mapped there based on interpretation of aerial photographs (Research Group for Active Faults 1980, 1991). After the Tohoku-Oki earthquake, many shallow normal-faulting earthquakes occurred in the southern Abukuma Mountains, of which the largest and most damaging was the Iwaki earthquake ( $M_w$  6.6) of 11 April 2011. Two known active faults, the Itozawa and Yunodake faults, ruptured simultaneously in that event (Mizoguchi et al. 2012; Toda and Tsutsumi 2013), and the subsurface seismogenic faults were inferred to be splay faults with steep dips through most of the seismogenic zone (Fukushima et al. 2013). Paleoseismic studies estimated recurrence intervals (based on the most recent and penultimate surface rupturing events) of 800–5900 years for the Yunodake fault (Miyashita 2018) and > 12,000 years for the Itozawa fault (Toda and Tsutsumi 2013; Niwa et al. 2013). These are much longer than

the recurrence interval of 500–700 years for the megathrust earthquake supercycle along the Japan Trench (e.g., Satake and Fujii 2014; Satake 2015; Sawai et al. 2015; Usami et al. 2018). No historical destructive inland earthquakes had been recorded before the 2011 Iwaki earthquake in the southern Abukuma Mountains (Usami 2013).

Our study area is northwest of Takahagi city in northern Ibaraki Prefecture, ~25 km south of the Iwaki earthquake rupture area (Fig. 1). This area also experienced normal-faulting earthquake swarms after the Tohoku-Oki earthquake, including the two events ( $M_w$  5.8 on 19 March 2011 and  $M_w$  5.9 on 28 December 2016) treated in this paper. Differential InSAR analyses detected distinct surface displacement associated with the 2011 event (Kobayashi et al. 2011; Fukushima et al. 2018) and the 2016 event (Fukushima et al. 2018) with relative surface displacements exceeding ~30 cm. The fault models derived from analyses of InSAR and global navigation satellite system (GNSS) data were 69.3° dip, –82.3° rake for the 2011 event and 77.8° dip, –80.3° rake for the 2016 event, meaning that the same fault plane was activated twice in less than 6 years (Fukushima et al. 2018).

Our study area is characterized by mountainous terrain reaching 500–800 m elevation (Fig. 1). The area is mainly underlain by Cretaceous granitoid and metamorphic rocks (Kubo et al. 2007), and rivers in the area such as the Ookita, Sekine, and Hananuki Rivers, flowing east toward the Pacific Ocean, do not appear to be controlled by geological boundaries (Additional file 1: Fig. S2). Although aerial photographs are interpreted as showing presumably active faulting to the west of the study area in the Tanakura tectonic belt and to the east of the study area in the Takahagi segment (Imaizumi et al. 2018), no active faults have been recognized within the study area (Fig. 1).

### Methods

#### InSAR analysis

To analyze coseismic and postseismic crustal deformation and fault behavior associated with the 2011 and 2016 earthquakes, we made maps of the line-of-sight (LOS) offset from the unwrapped InSAR phase data for the 2011 event, the 2016 event, and a 70-day period after the 2016 event (29 December 2016 to 9 March 2017). Original interferograms were produced from data recorded by the Phased Array-type L-band Synthetic Aperture Radar (PALSAR) instrument aboard the Advanced Land Observing Satellite (ALOS) for the 2011 event and from data recorded by PALSAR-2 aboard ALOS-2 for the 2016 event (details in Table 1). PALSAR data were observed in fine beam single mode (~10-m resolution) and PALSAR-2 data were observed in StripMap mode 1 (~3-m resolution). We were unable to assess postseismic

**Table 1** InSAR information used in this study

	Sensor	Path	Frame	Looking direction	Incidence angle (°)	Orbit	Date
2011 event							
Master	PALSAR	404	720	Right	38.7	Ascending	2011/02/02
Slave	PALSAR	404	720	Right	38.7	Ascending	2011/03/20
2016 event							
Master	PALSAR-2	18	2870	Right	36.1	Descending	2016/11/17
Slave	PALSAR-2	18	2870	Right	36.1	Descending	2016/12/29
Post 2016 event							
Master	PALSAR-2	18	2870	Right	36.1	Descending	2016/12/29
Slave	PALSAR-2	18	2870	Right	36.1	Descending	2017/03/09

deformation after the 2011 event because PALSAR stopped gathering data 2 months after the 2011 event and PALSAR-2 did not start operating until 2014.

The LOS offset map of the 2011 event was produced using GAMMA software (GAMMA Co. Ltd.), and the two 2016 maps were produced using RINC software (Ozawa et al. 2016). Noise reduction and phase unwrapping were based on the procedure of Sato and Une (2016); namely, multi-looking of  $4 \times 4$  pixel fields in range and azimuth was done to reduce noise, then filtering (32-pixel scanning window; intensity 0.2) after Goldstein and Werner (1998) was adopted for the InSAR image. Phases of the InSAR images were unwrapped using SNAPHU software (Chen and Zebker 2002). We used 10-m DEMs produced by the Geospatial Information Authority of Japan (GSI) to eliminate the topographic effect. During noise reduction of the PALSAR-2 InSAR images, we estimated the atmospheric delay (Ozawa and Shimizu 2010) from the mesoscale (10-km mesh) numerical weather model from the Japan Meteorological Agency (<https://www.jma.go.jp/jma/kishou/known/whitep/1-3-6.html>). Although these LOS offset maps include the long-wavelength crustal deformation from the Tohoku-Oki earthquake, the relative displacement across the line of maximum offset is little affected. Additionally, the LOS offset maps for the 2011 and 2016 events contain deformation resulting from aftershocks that occurred between the mainshock and the time of the second (slave) InSAR image. We cannot remove this aftershock effect, but because both slave InSAR images were obtained about 1 day after their respective mainshocks, its influence can be neglected for purposes of this study.

The InSAR images revealed linear surface displacements in the LOS direction (Fujiwara et al. 2019) consistent with surface faulting (Fig. 2). When we measured relative displacement along cross sections perpendicular to these possible faults, we noted three types of displacement: a distinct surface displacement, herein called SD (Fig. 3a), a wider deformation zone without a distinct surface displacement, which we called a flexure displacement (FD) (Fig. 3b), and a complex displacement that combined SD and FD (Fig. 3c). These cross-section lines ranged in length from 2 to 4 km, similar to profile lengths adopted by previous studies (e.g., Milliner et al. 2015; Scott et al. 2018). Profiles were placed an average of 200 m apart along strike, but were spaced unevenly in an effort to avoid noisy locations. We determined total offsets with errors estimated by the minimum and maximum cases (Fig. 3) using ArcMap software (ESRI Co. Ltd.).

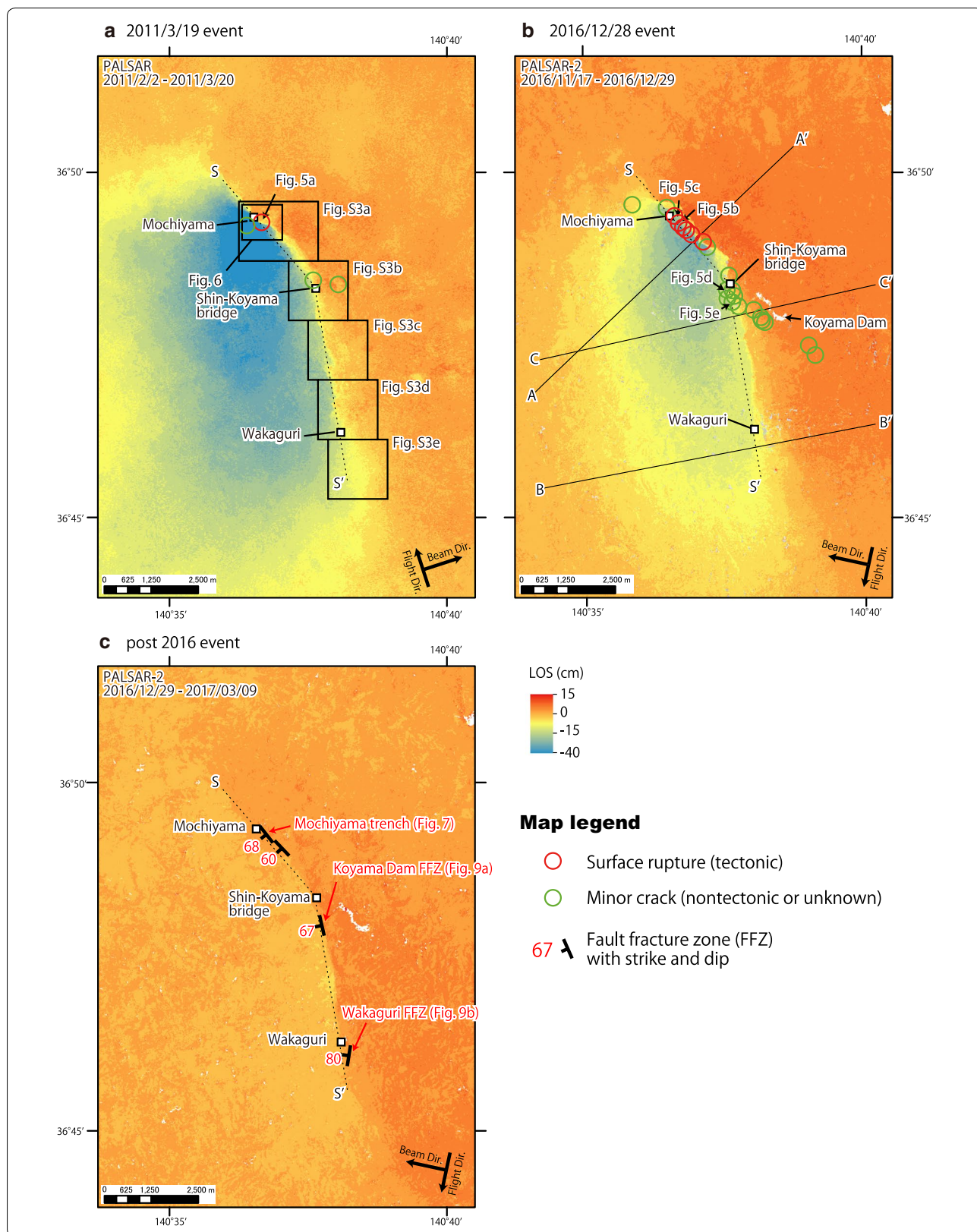
### Surface rupture mapping

To investigate coseismic surface ruptures associated with the 2011 and 2016 events and identify FFZs, we conducted field surveys on 19 April 2011; on 2, 7, and 16–18 January 2017; and on 22–24 February 2017. The 2011 survey was a 1-day reconnaissance that did not cover all areas along the linear surface displacements visible in the interferograms, but the 2017 surveys made an effort to cover the entire affected area.

We classified ruptures as tectonic, non-tectonic, or unknown. Tectonic ruptures originating from the seismogenic fault coincided with the linear surface displacement in InSAR images and were consistent with a fault

(See figure on next page.)

**Fig. 2** InSAR LOS maps of the study area (location in Fig. 1) showing surface deformation from **a** the 2011 event, **b** the 2016 event, and **c** the 70-day period after the 2016 event. Locations of tectonic surface ruptures (red circles) and non-tectonic or unknown minor cracks (green circles) found in field surveys are shown in **a** for the 2011 event and in **b** for the 2016 event. Profiles A–A', B–B', and C–C' in **b** are shown in Fig. 3a–c. Locations of FFZs and their strike and dip are shown in **c**



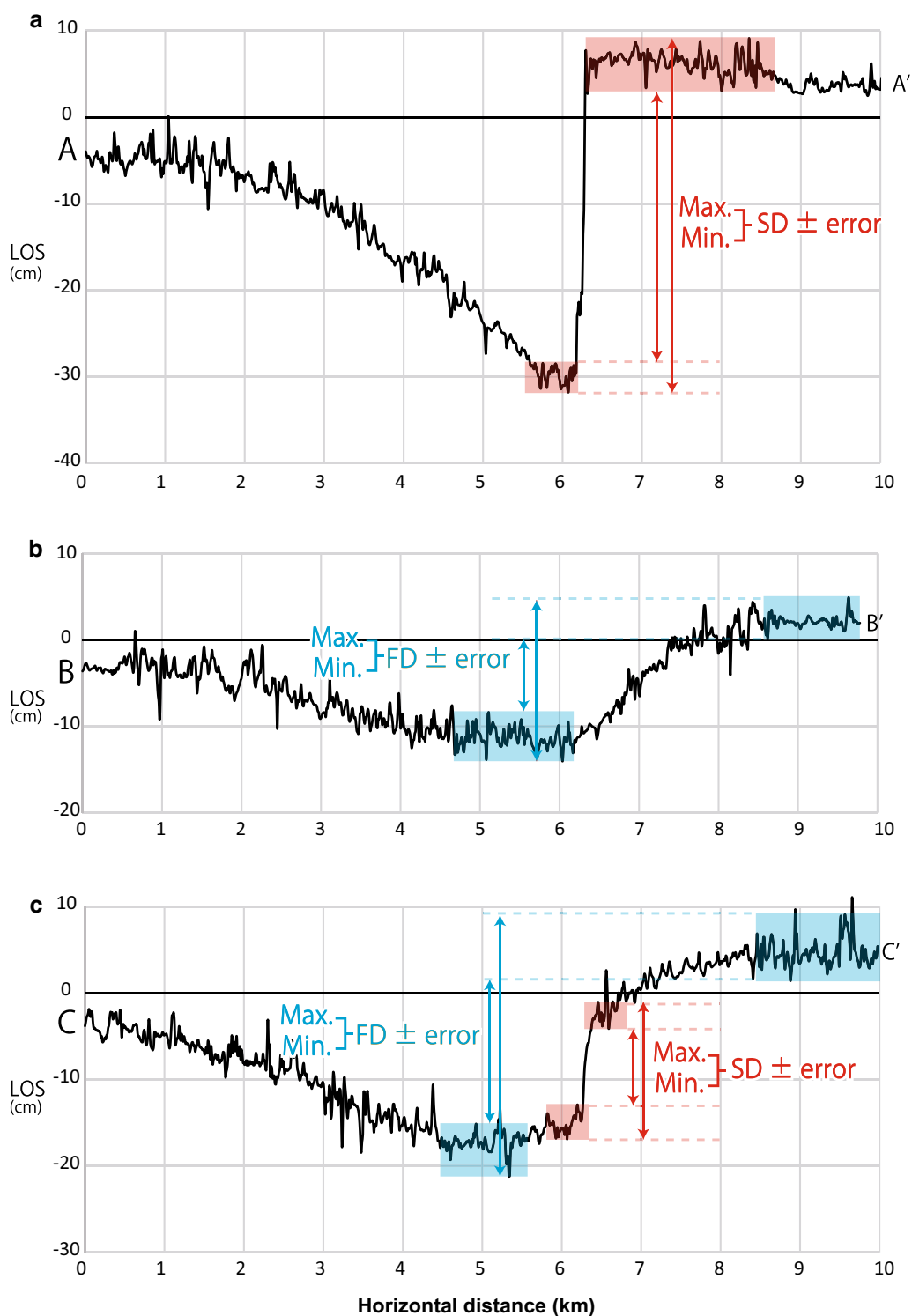


**Fig. 3** Profiles of LOS surface displacement from the 2016 event determined by differential InSAR analysis; locations are shown in Fig. 2b. **a** SD (surface displacement), **b** FD (flexure displacement), and **c** SD + FD (see text for definitions)

striking approximately NW–SE and dipping southwest, a model inferred by previous studies (Kobayashi et al. 2011; Fukushima et al. 2018). They also were generally more continuous than other ruptures and did not closely follow the local topographic relief. Surface displacements in soil and loose sediment were mapped as tectonic ruptures. On the other hand, we did not classify cracking, extension, and tilting of artificial structures (roads, bridges, and guardrails) as tectonic ruptures, even if they were concordant with a linear surface displacement, because these effects could arise from other types of deformation or from seismic shaking. The positions of ruptures were logged by GNSS using the mobile KASHMIR application (<https://www.kashmir3d.com/index-e.html>) with an error of a few meters.

#### Trench excavation and observation of FFZs

From 25 October 2017 to 18 January 2018, we excavated a trench near Mochiyama (the Mochiyama trench hereafter), where the 2016 earthquake produced a distinct surface rupture (Fig. 2b). The description of the trench walls was logged on gridded pages in a notebook at a scale of 1:10. After the first excavation and description, we further excavated the bottom of the Mochiyama trench to observe and log the deeper part. The final sketch log presented in this paper combines both logs.

After completing the description, we picked charcoal or wood fragments from the trench walls for radiocarbon dating. The dating was conducted at the Yamagata University high-sensitivity accelerator center in Yamagata, Japan. We conducted a Bayesian analysis (e.g., Biasi and Weldon 1994) by using OxCal software v.4.3.2 (Bronk Ramsey 2017) to calibrate radiocarbon ages to calendar years.

During the 2017 field surveys, we found some naturally exposed FFZs along the linear surface displacement. We observed and logged these FFZs and measured the dip, strike, and rake angles on the inferred latest fault plane.

#### Geomorphic interpretation

Our initial geomorphic observations were based on aerial photographs, including 1:20,000-scale black and white photographs taken in 1966 and 1:10,000-scale color photographs taken in 1975 by GSI. However, we failed to identify any tectonic geomorphic features in the study area, presumably because dense forest canopies made their detection difficult. We, therefore, used a lidar DEM covering the areas of linear surface displacement to seek such features. The original DEM data were obtained in 2012 (between the 2011 and 2016 events) by the Geological Survey of Japan, AIST, and have a resolution of 2 m (Yoshimi 2014). To help detect small geomorphic features, we used stereopaired morphometric protection

index red relief image maps (MPI-RRIMs) made from the lidar DEM using the stereo MPI-RRIMs Calculator software package (Kaneda and Chiba 2019).

## Results

### LOS offset maps and slip distributions of the 2011 and 2016 events

The LOS offset maps cover the same area for the 2011 event, 2016 event, and post-2016 event period (Fig. 2). There is a difference of  $2.6^\circ$  in incidence angles between the PALSAR and PALSAR-2 data (Table 1). Given a vertical offset of  $x$  (Additional file 1: Fig. S1), this difference is  $x \cos 36.1^\circ - x \cos 38.7^\circ$ , or  $\sim 2.7\%$ . That is, in the case of a vertical offset of 100 cm, the error resulting from this difference in LOS values would be  $\sim 2.76$  cm, which is acceptable in comparison to other sources of noise.

The LOS offset maps of the 2011 and 2016 events (Fig. 2a, b) show nearly identical curvilinear surface displacements extending about 10 km from northwest of Mochiyama past the Shin-Koyama bridge to southeast of Wakaguri. The line for the 2011 event is slightly longer than the line for the 2016 event, and the area of subsidence of the 2011 event, on the southwest side of the linear surface displacement, is also larger than that of the 2016 event. In both maps, the offset is greatest in the northern part of the area of subsidence.

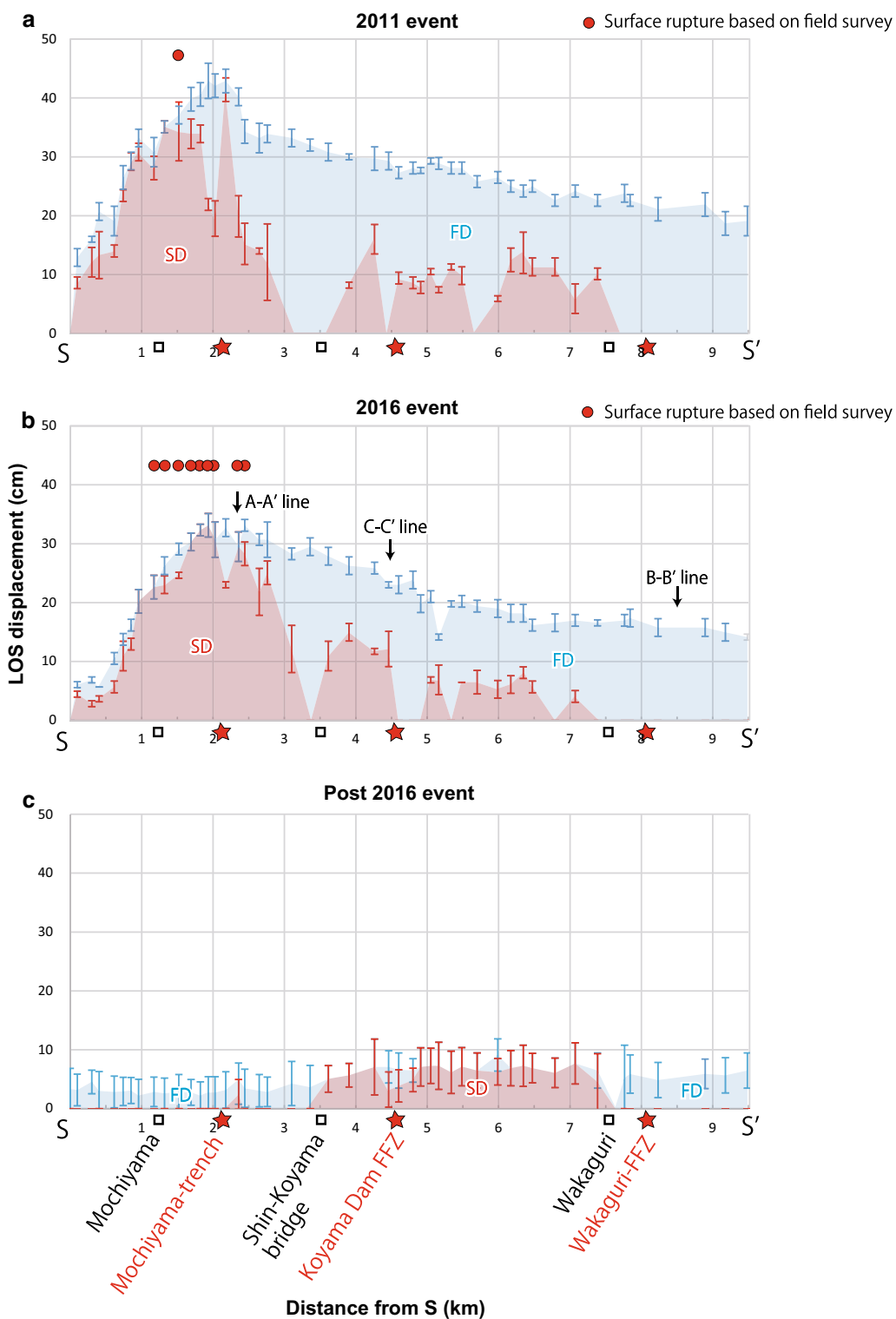
The post-2016 event LOS offset map (Fig. 2c) documents after slip deformation west of the linear surface displacement, but the area of greatest deformation is farther south than in the two earlier maps.

Figure 4 summarizes the distribution of relative LOS displacements along the linear surface displacement (approximated by line  $S-S'$ ) for the three mapping periods. We were able to separate the LOS displacement into SD and FD types.

The maximum relative LOS displacement in the 2011 event was  $\sim 43$  cm about 2 km from point S (Fig. 4a). From there, the displacement decreased steeply to the northwest toward point S and decreased more gently to the southeast toward point  $S'$ . Line  $S-S'$  was characterized by SD from 0 to 1.9 km, by SD+FD from 1.9 to 7.8 km (in which SD was intermittent), and by FD beyond 7.8 km (Fig. 4a).

The distribution of LOS displacement for the 2016 event (Fig. 4b) was very similar to that of the 2011 event. The maximum relative LOS displacement, also about 2 km from point S, was  $\sim 33$  cm, or  $\sim 10$  cm smaller than that of the 2011 event. Line  $S-S'$  was characterized by SD from 0 to 2.8 km, by SD+FD from 2.8 to 7.4 km (in which SD was intermittent), and by FD beyond 7.4 km (Fig. 4b).

The relative LOS displacement during the post-2016 event period was evenly distributed along line  $S-S'$  and



**Fig. 4** Distribution of relative displacement along line S–S' (location in Fig. 2a–c) based on LOS offset maps for **a** the 2011 event, **b** the 2016 event, and **c** the post-2016 event period. Red shading and error bars represent SD and blue shading and error bars represent FD. Red circles are locations of tectonic surface ruptures along line S–S'. The position of cross-section lines (Figs. 2b, 3) are also shown in **b**



was nowhere greater than 10 cm (Fig. 4c). Displacement was characterized by FD at both ends of line S–S' and by SD between 3.5 and 7.8 km.

#### Coseismic surface ruptures of the 2011 and 2016 events

Our field surveys after both earthquakes documented intermittent surface ruptures along the linear surface displacement. The LOS offset maps in Fig. 2a and b are annotated with colored symbols showing the locations of surface ruptures and their interpreted origin (tectonic, non-tectonic, or unknown). KML files with the locations of these surface ruptures are available in the electronic version of this paper (Additional file 2).

An asphalt road on the linear surface displacement near Mochiyama, where the largest relative LOS displacement occurred, was disrupted by the 2011 event (Fig. 5a). Although this damage affected an artificial structure, we assigned it a tectonic origin because of its position on the linear surface displacement and because clear surface ruptures continued beyond both ends of the damage zone on the road. After the 2016 event, the road was disrupted again and pre-existing cracks had clearly expanded (Fig. 5b).

In the 2017 surveys, we documented a clear and continuous open crack, not following the local topographic relief, around Mochiyama (Fig. 5c). The crack extended ~1.5 km length (Fig. 2b) and coincided with the area of peak relative LOS displacement (1–2.5 km from point S; Fig. 4b). However, the vertical displacement measured directly on this crack was nowhere greater than ~10 cm, whereas relative LOS displacement (total of the type of SD and FD) at this location was greater than 20 cm (Fig. 4b), suggesting that more than half of the actual vertical displacement took place off the fault trace. Crustal displacements derived from geodetic methods such as optical correlation of aerial photographs (e.g., Milliner et al. 2015) and differential lidar (e.g., Ishimura et al. 2019) usually indicate the total slip on the underlying seismogenic fault, including displacement accommodated by flexure, splay faulting, and tapering, and InSAR analysis is no exception (Scott et al. 2019). Therefore, our field measurements of the rupture are not considered to be anomalous.

We also found many minor cracks on artificial structures around the Shin-Koyama bridge, at the inflection point of line S–S' (Fig. 3b). We found evidence of two separate extension events on the Shin-Koyama bridge and a guardrail (Fig. 5d, e), which we attributed to the 2016 event and an earlier event. We found no ground ruptures or cracks south of the Shin-Koyama bridge along line S–S' (Fig. 2b). Some minor cracks were found outside the surface linear displacement around the

Koyama Dam (Fig. 2a, b) that appeared to be of non-tectonic origin, probably from local mass movement triggered by coseismic shaking.

#### Characteristics of tectonic geomorphic features

Our examination of MPI-RRIMs revealed small notches (subtle uphill-facing scarps) in ridge crests and subtle wind gaps coinciding with the linear surface displacement (Fig. 6 and Additional file 1: Fig. S2). Their detailed positions are shown in Additional file 1: Fig. S3.

All of the small notches are on slopes facing northeast to east and indicate subsidence toward the uphill side, consistent with tectonic movements like the 2011 and 2016 movements. However, these tectonic features were not found on fluvial terraces (Additional file 1: Fig. S2), leaving us unable to reliably document the Holocene activity on this fault from geomorphic observations. We describe these tectonic features from northwest to southeast along the linear surface displacement.

Near the northwest end of the linear surface displacement (Additional file 1: Fig. S3a), four notches on ridge crests were distributed along the right bank of a river. Two of these notches coincided with the 2016 surface ruptures (Fig. 6). A small bulge was recognized on a fluvial terrace northwest of the trench, but we cannot conclude that it has a tectonic origin because its shape is partly defined by a subtle gully on its southwest side that may represent a stream paleochannel (Fig. 6).

We did not identify any notches on ridge crests around the Koyama Dam, where some 2016 minor cracks were found (Additional file 1: Fig. S3b).

Farther south in the central part of the linear surface displacement, seven clear and well-aligned notches were found on ridge crests (Additional file 1: Fig. S3c). Their alignment strongly suggests a tectonic process rather than local mass movements, and their westward scarp orientation agrees well with the slip direction of the 2011 and 2016 events. However, our field surveys found no surface rupture around these notches. The area with notches corresponds to the area of postseismic deformation after the 2016 event shown by LOS displacements (Fig. 4c).

The area just north of Wakaguri (Additional file 1: Fig. S3d) contained only one wind gap. However, the adjoining area at the south end of the linear surface displacement contained several aligned notches and wind gaps on ridge crests (Additional file 1: Fig. S3e). Our 2017 surveys found no coseismic surface ruptures or minor cracks in either area, and relative LOS displacements indicated only FD in both areas in 2011, 2016, and the post-2016 event period (Fig. 4).

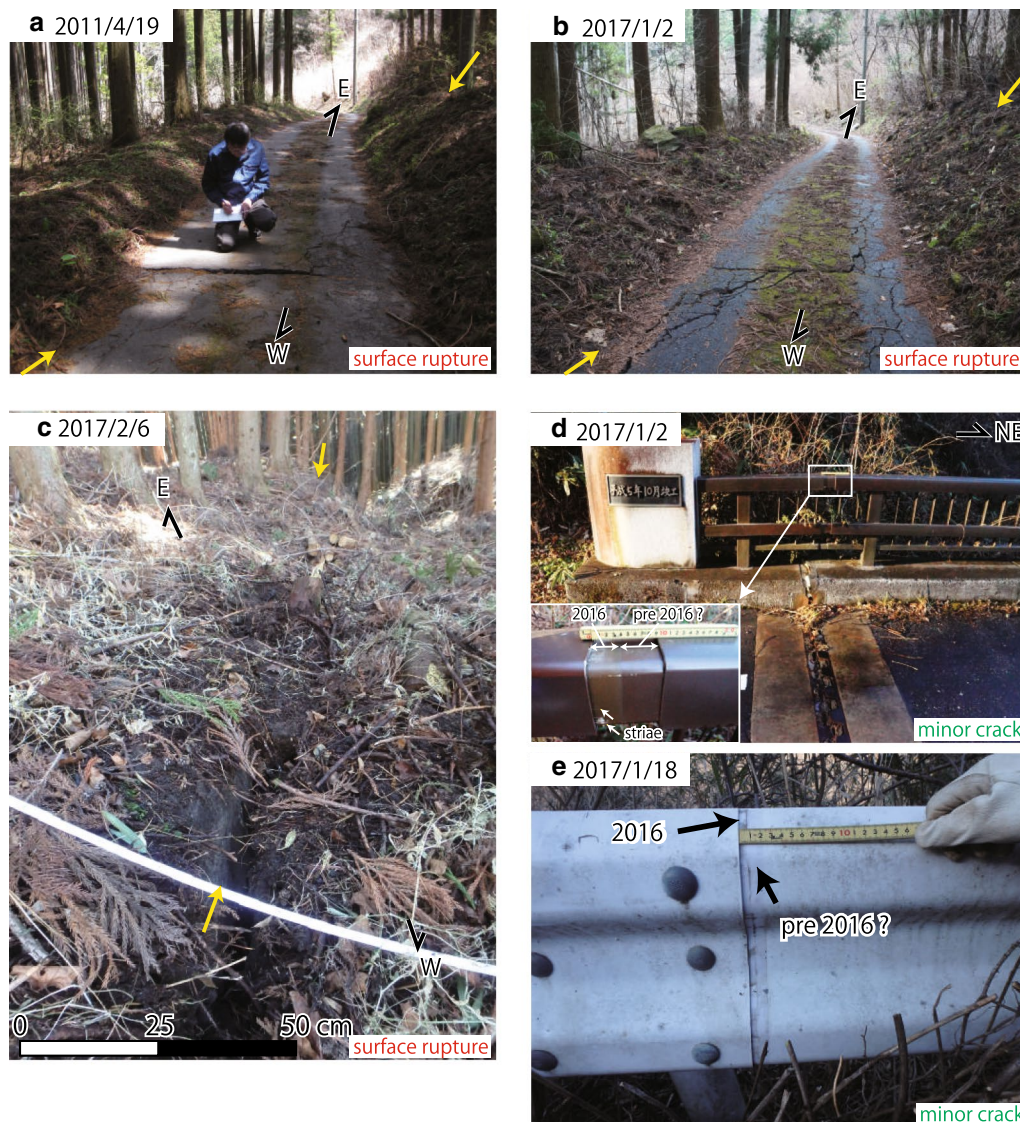


**Fig. 5** Photographs of surface ruptures; locations in Fig. 2a, b. Yellow arrows show the inferred fault trace based on the ruptures and linear surface displacement of InSAR analysis. **a** Damage in an asphalt road near Mochiyama 1 month after the 2011 event. **b** Further damage at the same location 5 days after the 2016 event. The total extension was measured as 12–13 cm, but this may include extension from the 2011 event. **c** Open crack after the 2016 event near Mochiyama in the area of peak LOS displacement, showing slight southwest-down displacement. **d** Extension across the Shin-Koyama bridge after the 2016 event. Although we had not checked the Shin-Koyama bridge in the 2011 survey, the pattern of weathering in the exposed steel implies extension in a pre-2016 event, presumably the 2011 event. The fresh and weathered zones measured 4 cm and 5 cm, respectively. **e** Evidence of extension in a guardrail at the Shin-Koyama bridge after the 2016 event. Fresh and weathered zones measured 0.8 cm and 1.6 cm, respectively

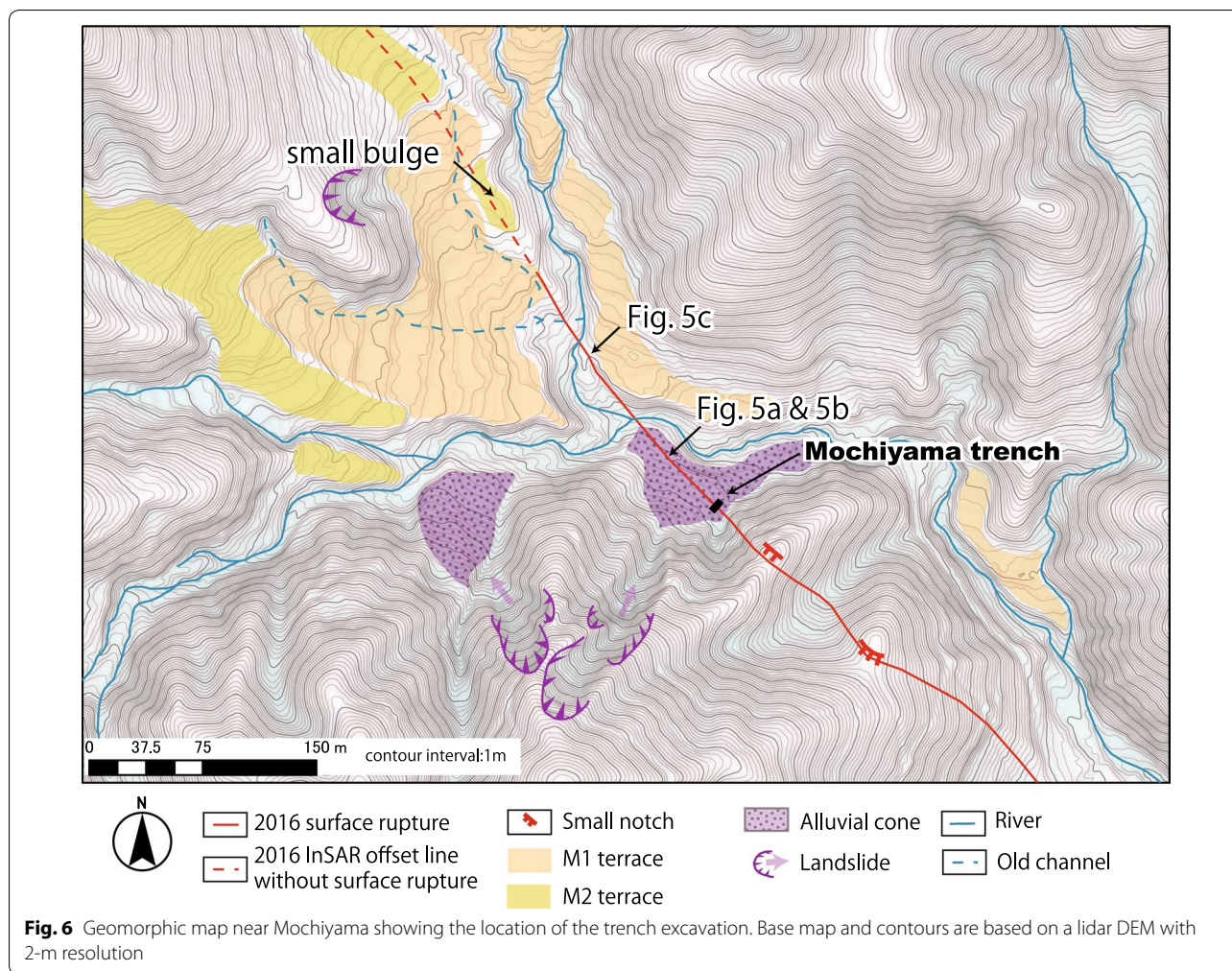
**Trenching on the 2016 surface rupture**

**Trench site and stratigraphy**

We conducted a trench excavation across the 2016 surface rupture near Mochiyama (36°49'15"N, 140°36'39"E) at a site where the largest surface ruptures occurred in the 2011 and 2016 events (Fig. 4a, b). Based on the DEM interpretation, the trench site is on a small alluvial cone on the right bank of the river, and small notches were

recognized on ridge crests southwest of the site (Fig. 6).

The surface rupture was in soft fine-grained soil in a *Cryptomeria* plantation and had an uphill-facing scarp with a maximum vertical displacement of ~10 cm, but this may have included displacement from the 2011 event as well as the 2016 event. We excavated a trench 4.0-m long, 2.0-m wide, and 2.5-m deep with nearly vertical



(75°) walls (Additional file 1: Fig. S4a) between October and December 2017.

Our sketch logs of the east wall and west wall are shown in Fig. 7a and b, respectively, and photomosaics of both walls are shown in Additional file 1: Fig. S5.

In descending order, the walls expose artificial forest soils, alluvial sandy deposits, gravel layers, and bedrock with a clear SW-side-down offset. The bedrock profile in the west wall is ~1.0-m deeper than in the east wall, suggesting that the bedrock surface dips toward the west. This vertical difference of 1.0 m measured across a trench 2.0-m wide suggests that the overlying sediment inclines by 25°–30°. We divided the overlying sediments into more than 20 stratigraphic units on the basis of their facies and continuity. The exposed bedrock is strongly weathered biotite-rich granodiorite.

The faults that reached the ground are interpreted as normal faults because splay faults and open fissures are well developed on the footwall side (northeast). The ground is offset as much as ~10 cm in the east wall,

but offset in the west wall is unclear because the faults spread apart more widely than in the east wall, perhaps reflecting the difference in the thickness of the overlying sediment. The splay faults in the east wall converge at ~0.8-m depth (Fig. 7a), whereas the faults in the west wall become obscure with depth (Fig. 7b). Convergent faults in both walls tend to dip 60°–70° toward the northeast. A void in the east wall along the fault, which was about 0.3-m wide and 1.2-m high when we started logging, gradually enlarged during the excavation as gravel continued to fall from the hanging wall (southwest) side, which supports extensional or subsidence stress due to normal faulting or a possibility making as if faulting continued during excavation. The apparent offset of bedrock along the fault, as measured in the field, is as great as 35 cm. Considering the 75° inclination of the trench wall (Additional file 1: Fig. S4a) and the 60°–70° dip of the fault, the vertical offset of the bedrock is estimated as 25–30 cm in the east wall (inset of Fig. 7a), whereas 19 cm of apparent

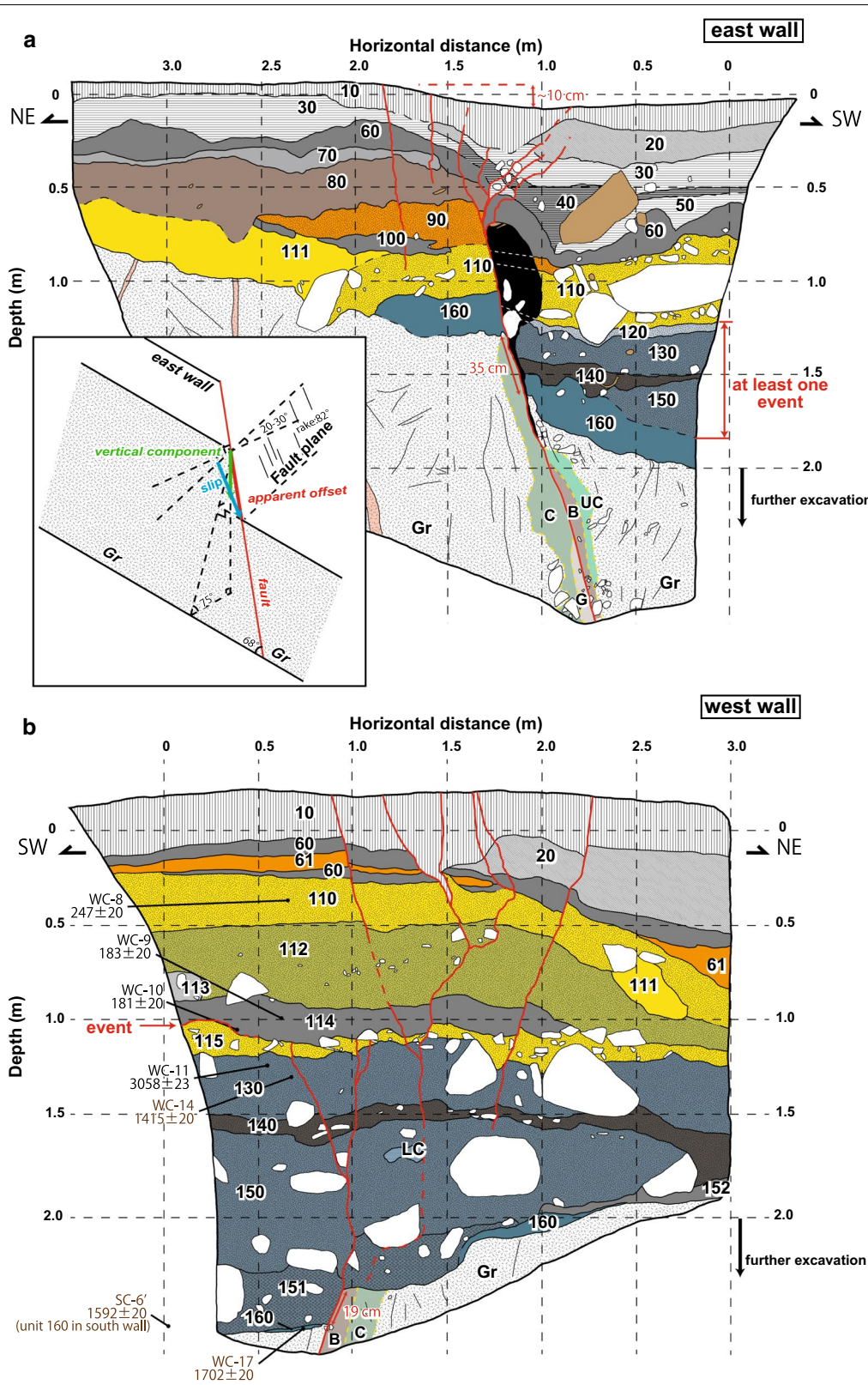


**Fig. 7** Sketch log of **a** the east wall and **b** the west wall of the Mochiyama trench including radiocarbon ages (yr BP). Black lines are boundaries of sediment units and yellow-dashed lines are lithofacies boundaries within the bedrock

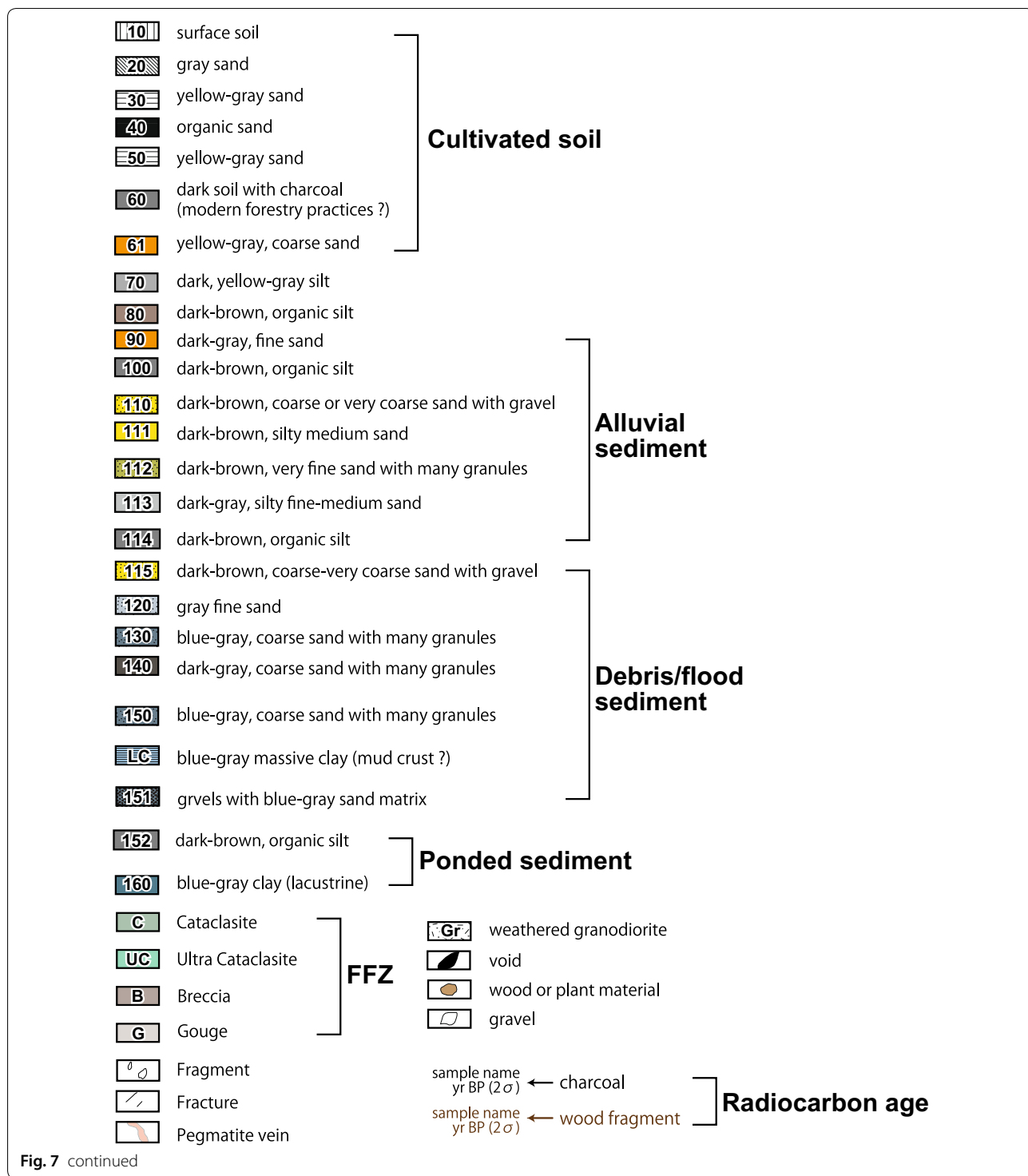


Fig. 7 continued

offset was measured in the west wall. The portion of the trench deeper than 2.0 m has vertical walls; therefore, the vertical offset of bedrock is estimated as 14–17 cm from the evidence in the west wall. The reason for this

difference of 8–16 cm in vertical offset between the east and west walls is unclear. Presumably, subsidiary fault(s) that compensate the difference may be hidden in the west wall or outside of the trench. Similar

branched faults or fault migration are also reported in sandbox models (Paul and Mitra 2015; Livio et al. 2019).

Units 20–50 consist of poorly sorted yellow-gray to gray sand that contains logs, charcoal, and trash. The organic sand and yellow-gray sand (units 40 and 50) occur only in the downthrown side of the east wall (Fig. 7a), and the overlying gray sand (unit 20) lies on opposite ends of the trench in the east and west walls. Unit 60, a dark soil containing abundant charcoal, and the interbedded yellow-gray sand (unit 61) in the west wall are interpreted as artificial deposits that are probably associated with modern forestry practices.

The underlying units 70–115 are mainly composed of dark brown and dark yellowish sand or sandy silt with abundant angular gravel. Units 70–100 are recognized only in the east wall (Fig. 7a), perhaps because the human activities associated with overlying units 30–60 removed them from the west wall. The sand units (units 110–113 and 115) present in both walls are interpreted as tributary sediments on an alluvial plain, although the dark brown organic silt (unit 114) intercalated within them in the west wall (Fig. 7b) suggests that tributary flow was interrupted at least once.

Units 120–151 consist of grayish sand with abundant angular gravel. These units (except for 120) cross all the faults in the west wall (Fig. 7b), but they appear only on the dropped side in the east wall, suggesting that elsewhere they were eroded away and replaced by overlying units 110 and 111 (Fig. 7a). These poorly sorted facies containing angular gravel are suggestive of debris-flow material rather than alluvial sediment. In the west wall, a lump of massive blue-gray clay (unit LC) within unit 150 is interpreted as a mud crust brought here from upstream.

Unit 160 is blue-gray clay with some visible plant material. It directly overlies the bedrock and is distinctly displaced by a fault in the east wall, but it is only intermittently present in the west wall (Fig. 7b). The fragmentary and inclined distribution of this unit suggests that it was eroded away during deposition of the overlying sand (unit 150). The abundance of clay implies a lacustrine rather than an alluvial or debris-flow sediment.

Our age control in the Mochiyama trench was based on seven radiocarbon ages of charcoal or wood fragments picked from the west wall plus one sample picked from the left side of the southern end wall of the trench (sample SC-6'). The sample locations and their ages in uncalibrated years (yr BP) are shown in Fig. 7b, and more details and calibrated ages are listed in Table 2.

The uncalibrated ages ranged from ~180 to ~3000 year BP. We conducted a Bayesian analysis using OxCal software to yield calibrated calendar years and check the consistency with the stratigraphic order, as shown in Fig. 8. Most of the calibrated ages were concordant with the stratigraphic order, but sample WC-11 yielded an age ~2000 years greater than the modeled stratigraphic order. Sample WC-11, a ~1-cm piece of charcoal in the blue-gray sand of unit 130, may be reworked material and was excluded from this study. Our results suggest that the upper units 10–114 are all less than 300 years old, which supports our observation that the units 10–61 are artificially disturbed soils and suggests that the underlying units 110–114 were also subjected to artificial disturbance. Additionally, a gap of more than 1000 years between the units 114 and 130 indicates that the upper part of unit 130 was eroded away during deposition of the overlying sand (unit 115) or by forestry practices.

**Table 2 Radiocarbon ages of the Mochiyama trench**

Sample name	Sample wall	Unit	Material	Pretreatment <sup>a</sup>	$\delta^{13}\text{C}$ (‰)	$^{14}\text{C}$ age (yr BP)	Calibrated age (2 $\sigma$ )	Lab number
WC-8	West wall	110	Charcoal	AAA	$-24.91 \pm 0.36$	$247 \pm 20$	1636–1670 AD (74.2%) 1780–1800 AD (21.2%)	YU-7142
WC-9	West wall	114	Charcoal	AAA	$-27.42 \pm 0.40$	$183 \pm 20$	1663–1685 AD (18.3%) 1733–1808 AD (55.4%) 1928 AD (21.7%)	YU-7143
WC-10	West wall	114	Charcoal	AAA	$-25.28 \pm 0.43$	$181 \pm 20$	1663–1685 AD (18.3%) 1731–1809 AD (55.4%) 1927 AD (21.7%)	YU-7018
WC-11	West wall	130	Charcoal	AAA	$-27.21 \pm 0.56$	$3058 \pm 23$	1404–1260 BC (94.6%) 1240–1236 BC (0.8%)	YU-7019
WC-14	West wall	130	Wood fragment	AAA	$-30.34 \pm 0.32$	$1415 \pm 20$	605–657 AD (95.4%)	YU-7144
WC-17	West wall	160	Twig	AAA	$-26.90 \pm 0.37$	$1702 \pm 20$	257–296 AD (17.8%) 321–397 AD (77.6%)	YU-7145
SC-6'	South wall	160	Twig	AAA	$-29.08 \pm 0.24$	$1592 \pm 20$	415–537 AD (95.4%)	YU-7146

<sup>a</sup> AAA indicates that NaOH concentration reached 1.0 mol/L in acid–alkali–acid pretreatment

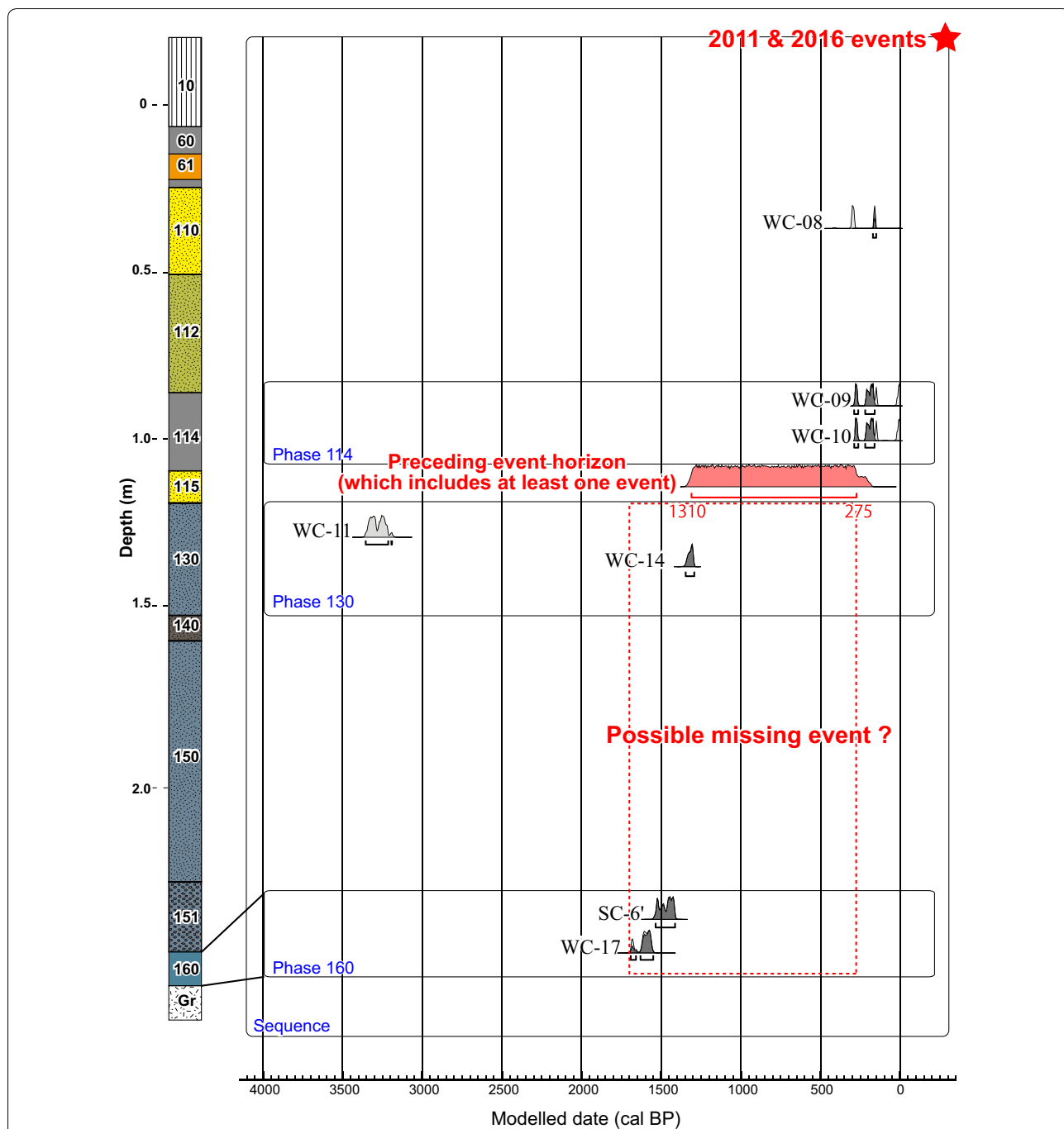


**Fig. 8** Age–depth plot showing the constrained probability density distribution of radiocarbon ages in a synthesized stratigraphic column of the west wall of the Mochiyama trench (Fig. 7b), made with OxCal v4.3.2 software (Bronk Ramsey 2017). Light-gray curves are the original probability density distribution of radiocarbon ages, and dark-gray curves are density distributions refined by Bayesian analysis. The red curve is the probability distribution of the age of the preceding event as constrained by radiocarbon ages. The blue outlines labeled “Phase” enclose all radiocarbon ages from each stratigraphic unit, and the outline labeled “Sequence” defines the order of events and groups of radiocarbon ages (Bronk Ramsey 2017)

### Paleoseismic evidence

In our trenching study, we could not distinguish the 2011 from the 2016 event in the most recent event horizon. However, both events must have affected the ground surface (surface of unit 10) because there were no artificial disturbances between 2011 and 2016.

In the east wall (Fig. 7a), the charcoal-rich dark soil (unit 60) appears to be displaced downward by more than 20 cm across the fault, but this offset is clearly unnatural because it exceeds the offset of underlying units 90 and 110. We infer that the unit 60 was deposited on a surface that sloped toward the southwest. The units 90 and 110 display apparent offsets of ~10 cm along the fault, whereas the unit 160 and bedrock are displaced by as much as ~35 cm, suggesting that at least one faulting event before 2011 occurred after the deposition of unit 160 but before unit 110 was deposited.

In the west wall (Fig. 7b), the 19 cm of apparent offset of bedrock along the fault plane appears to be the result of multiple faulting events besides the 2011 and 2016 events, because the individual offsets of branch faults on the upper surface of unit 114 total no more than ~10 cm. Additionally, the unit 114 itself truncates branches of the fault on the southwest side of the trench. These observations indicate that the splay faults in units 10–150 (on the northeast footwall side) are associated with the 2011 and 2016 events, but other splay faults in units 115 and lower (on the southwest hanging wall side) are associated with an event earlier than 2011. This “normal-fault migration” toward the footwall side is explained well by sandbox modeling (Paul and Mitra 2015; Livio et al. 2019). We infer that the last major faulting event before 2011 occurred just before the deposition of unit 114. The unit 114 is a dark-brown organic-rich silt that suggests a setting of temporary ponding, which is a typical environmental change that accompanies fault motion. However, the possibility that the unit 114 is a consequence of forestry practices cannot be ruled out because of its young age (~300 cal BP; Fig. 8). In any case, this event may be the same event we identified between the units 160 and 110 in the east wall.

We, thus, conclude that at least one offsetting event occurred before the 2011 event at the location of the Mochiyama trench. The radiocarbon ages from overlying unit 114 (samples WC-09 and WC-10) and underlying unit 130 (sample WC-14) suggest that this event occurred in 275–1310 cal BP (Fig. 8).

The exact offset associated with this preceding event is difficult to infer. In the east wall, the apparent along-fault offset of units 90 and 110, ascribed to the 2011 and 2016 events, is ~10 cm. Subtracting this from the ~35 cm offset of the bedrock leaves a remainder of ~25 cm, which seems to be a large offset for a single preceding event comparing to the 2011 and 2016 cases. In the west wall,

subtracting the offset of unit 114 (~10 cm) from the bedrock offset leaves a remainder of ~9 cm. In addition, the vertical displacement of units 115–140 seems to be smaller than the offset of bedrock. However, we did not recognize any other convincing evidence of paleoseismic events, such as stratigraphic changes or fault truncations within the units 120–150 in the east wall or units 115–160 in the west wall.

### Characteristics of FFZs

After logging the initial walls of the Mochiyama trench, we excavated deeper to investigate the detailed structure and characteristics of the FFZ within the bedrock. In addition, we found three naturally exposed FFZs along the linear surface displacement during our 2017 surveys. Figure 2c shows the location and fault parameters (strike and dip) of these FFZs, and details of the position are shown in the Additional file 1: Fig. S3 and Additional file 2. We observed and logged all of these FFZs except one that was on a dangerously steep slope.

### FFZ in the granodiorite exposed in the Mochiyama trench

The bedrock materials in the FFZ in the Mochiyama trench (Fig. 7) are categorized as layered gouge, breccia, cataclasite, and ultracataclasite as defined by Sibson (1977) and Takagi and Kobayashi (1996).

In the east wall (Fig. 7a), a breccia zone (unit B) on the southwest side of the fault increases to ~8 cm in width at the trench bottom. Below ~2.3-m depth, a zone of gouge (unit G) ~4-cm wide appears between the fault surface and the breccia. Fresh slickenlines on the northeast face of the gouge (Additional file 1: Fig. S4d) may represent the fault plane associated with the 2011 and 2016 events because its strike (N42°W), dip (68°W), and rake (82°S) angles are in rough agreement with the seismogenic fault model proposed by Fukushima et al. (2018).

The northeast (footwall) side of the main fault zone consists of mottled gray- and light-brown cataclasite (unit C) that grades into the intact rock (Fig. 7a). It is up to ~10-cm wide near the trench bottom. The breccia zone (unit B) on the southwest (hanging wall) side of the fault is bounded by ultracataclasite (unit UC).

In the west wall (Fig. 7b), no gouge is apparent along the fault. A band of breccia ~5-cm wide appears on the northeast side of the fault (unit B), whereas breccia is on the southwest side of the fault in the east wall. On the northeast (footwall) side of the breccia is mottled gray- and light-brown cataclasite (unit C), as in the east wall.

### Koyama Dam FFZ

The Koyama Dam FFZ (36°47′55″N, 140°37′45″E) is in a tributary valley on the right bank of Ookita River (Fig. 2c and Additional file 1: Fig. S3b), where it has been partly



exposed by the river (Additional file 1: Fig. S4b). Coseismic surface ruptures were not found near this area, but subtle cracks on a nearby asphalt road were noted during the 2017 field surveys. The LOS displacement distribution of both events suggests that SD+FD type deformation (Fig. 3c) occurred around this FFZ (Fig. 4a, b), whereas afterslip characterized by SD type (Fig. 3a) occurred after the 2016 mainshock (Fig. 4c). The lidar DEM revealed no tectonic geomorphic features in the vicinity (Additional file 1: Fig. S3b).

We removed surface soil to reveal an exposure 2-m long and 1.5-m wide that crosscuts the FFZ, and cleaned the FFZ for examination. The intact rock is hard granodiorite, less weathered than the bedrock in the Mochiyama trench. The exposed fracture zone is characterized by gray to green-gray colors. We categorized its materials as gouge, breccia, and cataclasite on the basis of its facies and fragmentation (Fig. 9a).

The central part of the fracture zone is gouge with an apparent thickness of ~20 cm. The eastern half is green and the western half is gray-brown. A zone of loose sediment within the overlying sediment (Fig. 9a) extends across the fault to the western edge of the gouge. The fresh slickenlines on the fault trace include one with a N6°W strike, 67°W dip, and 72°S rake angle (Additional file 1: Fig. S4e), which is roughly consistent with the seismogenic fault model of the 2011 and 2016 events. These findings suggest that the western edge of the gouge is the slip plane associated with the 2011 and 2016 events. Another notable feature is that the gray-brown gouge includes clayey fragments plucked from the green gouge (Additional file 1: Fig. S4f). This phenomenon cannot be explained by a single faulting event.

Breccia zones border the gouge zone on both sides. The breccia on the east side (green breccia) is 50–60-cm thick and contains light-brown rock fragments of mixed size in a blue-gray matrix. The breccia on the west side (green-brown breccia) is 10–15-cm thick and composed of incoherent light-gray fragmental material. Its outer edge grades into a zone of cataclasite 10–20-cm thick. The cataclasite grades into the granodiorite and partially retains its original structure.

#### **Wakaguri FFZ**

The Wakaguri FFZ (36°46′04″N, 140°38′10″E) is on the right bank of the Sekine River perpendicular to a slope undercut by the river (Fig. 2c and Additional file 1: Fig. S3e). We found no coseismic surface cracks or minor cracks near Wakaguri. This area was characterized by FD-type deformation from both events and the postseismic period in 2016 (Fig. 4), although aligned notches and subtle wind gaps on ridge crests are visible in the DEM on this part of line *S–S'* (Additional file 1: Fig. S3e).

We cleaned the FFZ and logged an exposure that was 0.5-m high and 1.5-m wide (Additional file 1: Fig. S4c). The intact rock is weathered granodiorite with some pegmatite veins on its east side. The fracture zone consists of a thin layer of gouge flanked by green breccia on one side and cataclasite on the other (Fig. 9b). All parts of this FFZ are thin compared to the Mochiyama trench and Koyama Dam FFZs.

The breccia zone is ~20-cm thick and is sharply bounded on both sides. The gouge zone is 0.5–1.0-cm thick and features poorly defined slickenlines with N10°E strike, 80°W dip, and 73°S rake angle (Additional file 1: Fig. S4g). Although this strike diverges slightly from that of the linear surface displacement, it is broadly consistent with the seismogenic fault model. Because the Wakaguri FFZ is near the south end of the area of coseismic deformation, splaying of the normal fault near its termination may account for the divergent strike. The subtle slickenline and LOS offset imply that slight movement may have occurred during the 2011 or 2016 event, or in past events, although no clear offset is apparent in the overlying sediment.

## **Discussion**

### **Comparison of surface ruptures of the 2011 and 2016 events**

Our LOS displacement maps show that the 2011 and 2016 events have similar distribution and discontinuity of ground deformation (Fig. 2a, b) and similar distributions of LOS displacement (Fig. 4a, b), and in all these respects the 2011 event was slightly larger than the 2016 event. Surface ruptures of both events were found in the same locations in the Mochiyama region (Fig. 5a, b), and some artificial structures were damaged by both events (Fig. 5d, e). These findings, along with the clear offsets of bedrock, slickenlines, and layered FFZs including gouge along the linear surface displacement, confirm the tectonic origin of these features by displacement on the Mochiyama fault. We defined the detail of the Mochiyama fault based on the distribution of tectonic surface ruptures, notches, and FFZs. The fault is at least ~8-km-long curvature-shaped trace from the northern tip of 2016 surface rupture (36°49′25″N, 140°36′32″E) to the southern tip of notches (36°45′27″N, 140°38′11″E). After the measurements of fault plain within the FFZs, we also defined the average fault parameters of 60°–70°W dip, N42°W–N45°W strike of the northern part and 70°–80°W dip, N6°W–N10°E strike of the southern part. The KML file of trace is available in Additional file 2.

The similarity in the LOS displacement distributions and damage to artificial structures from the two events supports the suggestion by Fukushima et al. (2018), based on InSAR analysis and GNSS data, that the fault

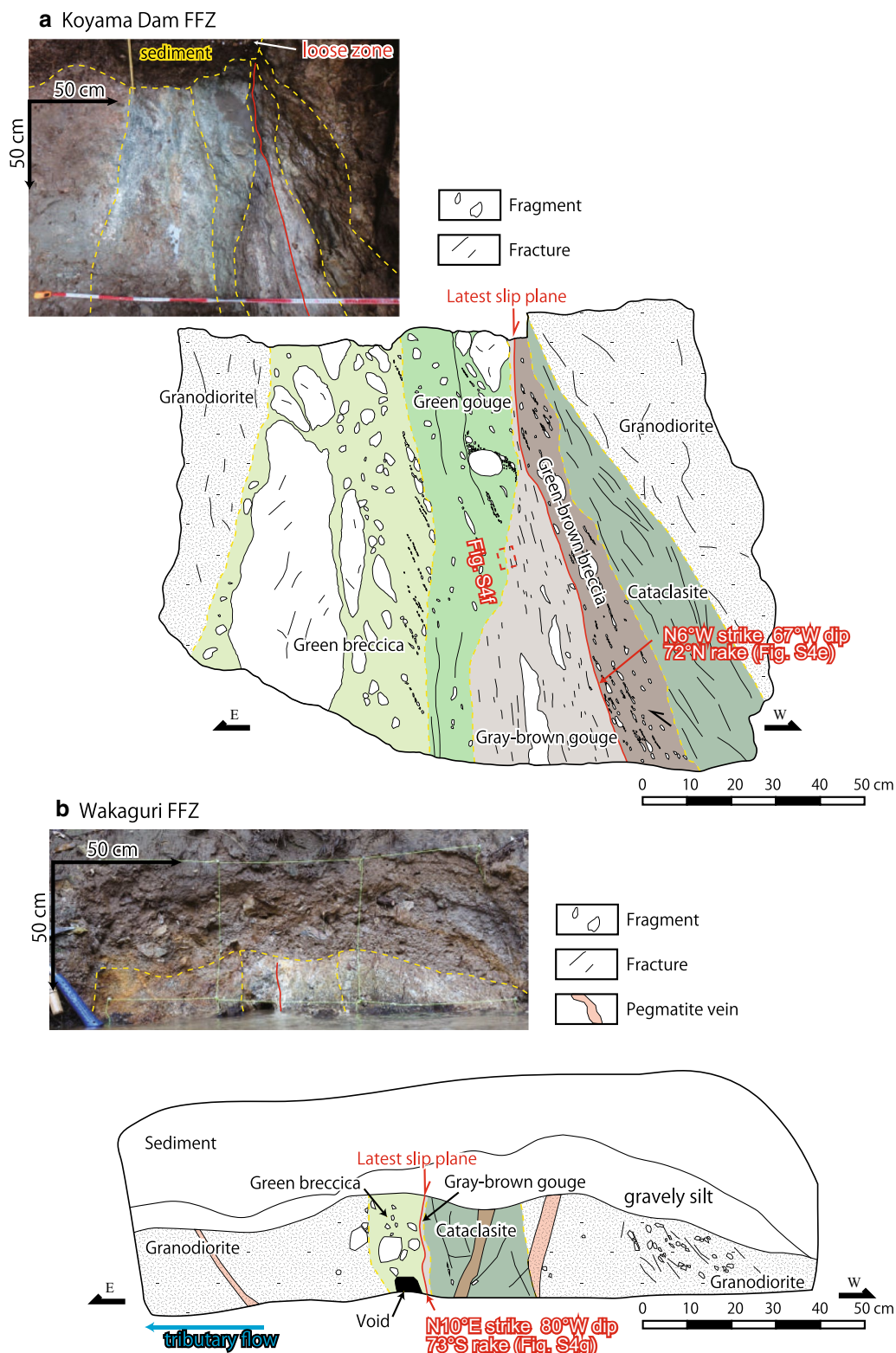


**Fig. 9** Photograph and sketch log of **a** the Koyama Dam FFZ (see Fig. 2c and Additional file 1: Fig. S3b for location) and **b** the Wakaguri FFZ (see Fig. 2c and Additional file 1: Fig. S3e for location). Yellow-dashed lines indicate boundaries of lithofacies in bedrock

surface of the 2011 event was reactivated in 2016. The similarity in the distribution of the coseismic LOS displacement, along with the slight disparity in the effects of the two events, is consistent with semicharacteristic slip behavior (Kaneda and Okada 2008) rather than characteristic slip behavior (Schwartz and Coppersmith 1984). This is the first case to our knowledge in which semicharacteristic behavior of a normal fault has been revealed by remote sensing techniques.

Other cases of successive ruptures matching the patch model of Sieh (1996) have been reported from central Italy in a normal fault system. The partial rupture of the northwest part of the Paganica–San Demetrio fault in the 2009 L’Aquila earthquake (Civico et al. 2015) is consistent with the patch model. And the 2016 Norcia and Amatrice earthquake sequences, which occurred two months apart, reactivated the same fault plane but differed in their scales and slip distributions (Villani et al. 2018; Ferrario and Livio 2018; Brozzetti et al. 2019). These observations suggest that normal faults may tend to respond irregularly to regional extensional stress. In any case, the examples cited here indicate that classical models of recurrence and slip behavior should be updated. The InSAR techniques that enabled us to characterize fault behavior in events of moderate magnitude in this mountainous region will be valuable here and elsewhere for studying subsidiary fault behavior.

**Comparison of paleoseismic history with the Yunodake and Itozawa faults**

The paleoseismic histories of normal faults in the southern Abukuma Mountains that were triggered by the Tohoku–Oki earthquake are an important aspect of the

interaction between megathrust earthquakes and inland stress changes. Published examples include the evidence of inland triggered earthquakes associated with the AD 1454 Kyotoku ( $M_w > 8.4$ ; Sawai et al. 2015) and AD 869 Jogan earthquakes ( $M_w > 8.6$ ; Namegaya and Satake 2014), considered the two most recent megathrust events before the 2011 Tohoku–Oki earthquake (e.g., Satake and Fujii 2014; Satake 2015; Usami et al. 2018). In the case of the 2011 Iwaki earthquake, which ruptured both the Yunodake and Itozawa faults, Miyashita (2018) reported that the Yunodake fault ruptured in 5900–6700 cal BP and 800–6200 cal BP and suggested that the later event could have been synchronous with the AD 869 Jogan earthquake. On the other hand, Toda and Tsutsumi (2013) found no evidence that the Itozawa fault ruptured in association with the AD 1454 Kyotoku or AD 869 Jogan events, but instead reported evidence of surface faulting in 12,620–17,410 cal BP.

Our trenching study found that at least one event, including the penultimate faulting event on the Mochiyama fault, occurred in 275–1310 cal BP. The age of that event is consistent with both the AD 1454 Kyotoku and AD 869 Jogan earthquakes in the Japan Trench (Fig. 10). The age range of that event overlaps with an event on the Yunodake fault with an age range of 800–1310 cal BP, suggesting the possibility of simultaneous earthquakes on the Yunodake and Mochiyama faults. To evaluate this possibility, we calculated Z statistics (e.g., Sheppard 1975; McCalpin 2009), a quantitative method to compare the overlap of the two ages given their means and standard deviations. The mean ages and standard deviations of the penultimate events are  $3500 \pm 2700$  years for the Yunodake fault and  $792.5 \pm 517.5$  years for the Mochiyama fault. The calculated Z statistic for both

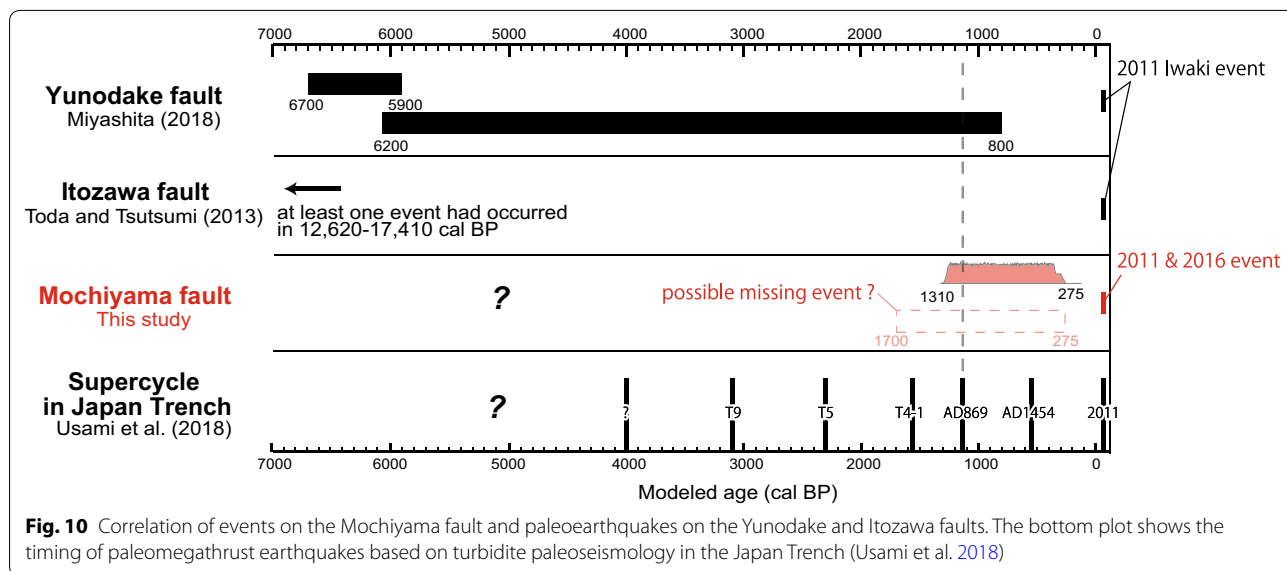


**Fig. 10** Correlation of events on the Mochiyama fault and paleoearthquakes on the Yunodake and Itozawa faults. The bottom plot shows the timing of paleomegathrust earthquakes based on turbidite paleoseismology in the Japan Trench (Usami et al. 2018)

events is 0.98, or a probability of ~35% that these events were synchronous. If they occurred in 800–1310 cal BP, they could correspond to the AD 869 Jogan megathrust earthquake, but not the AD 1454 Kyotoku earthquake or the T4-1 earthquake of ~1500 cal BP (unknown magnitude; Fig. 10) inferred from tsunami deposits in the Sendai plain (Sawai et al. 2012) and turbidites in the Japan Trench (Usami et al. 2018). Of course, a possibility cannot be ruled out that the Mochiyama fault ruptured in association with the AD 1454 event or was triggered by the T4-1 earthquake, while the Yunodake fault was not activated at those times. An important possibility from the paleoseismology of the Abukuma Mountains is that the case of 2011, in which the Yunodake, Itozawa, and Mochiyama faults all ruptured, is a rare occurrence in the supercycle of the Japan Trench. Further paleoseismic studies are needed, in the Abukuma Mountains and elsewhere in megathrust regions, to elucidate the relationships, if any, between triggered reactivation of inland faults and megathrust supercycles.

#### Detection and assessment of slow slip-rate faults

The tectonic geomorphic features on the Mochiyama fault escaped detection in aerial photos until the fault produced earthquakes. It took our observations of a DEM to find these subtle features. This case presents an example of an active fault near the threshold of geomorphic detectability, at which the slip rate is only slightly greater than the local denudation rate. Kaneda (2003) suggested that the threshold slip rate at which detectable geomorphic signs are produced in humid granitic mountain regions is ~0.1 mm/year. Fujiwara et al. (2001) reported average basin-scale denudation rates of ~0.132 mm/year in the Abukuma Mountains based on the relationship between sediment delivery rates to reservoirs and the dispersion of elevation. Nakamura et al. (2014) estimated denudation rates in the Abukuma Mountains of 0.114–0.180 mm/year based on the concentration of cosmogenic nuclides in fluvial sediments. Although we cannot discuss the slip rate of the Mochiyama fault directly due to lack of cumulative offsets on fluvial terrace or alluvium, these previous studies suggest that the slip rate of the Mochiyama fault is no greater than ~0.1 mm/year. If an offset of 10–20 cm occurred in every earthquake, which is the combined offset of the 2011 and 2016 events based on the offset of bedrock in the Mochiyama trench, then the estimated cumulative recurrence interval would be 1000–2000 years or longer. This evidence also supports the inference that the Mochiyama fault has not always been triggered in synchrony with the Japan Trench earthquake supercycle (500–700 years), but we

should investigate slip rate of the fault directly in some method, for example by the aligned coring across the fault.

Our field surveys located FFZs along the Mochiyama fault that were possibly activated in both the 2011 and 2016 events. These were characterized by distinct and layered fracture zones including plucked clay fragments (Additional file 1: Fig. S4f). Aiyama et al. (2017), observing the active Yamada fault in a granitic outcrop in central Japan, described layered gouge zones within the FFZ; whereas inactive minor faults in the same outcrop were in direct contact with cataclasite and not associated with gouge. At the active trace of the Nojima fault in central Japan, layers of gouge in granite have been explained by repetitive faulting at shallow crustal levels (Shigetomi and Lin 1999; Otsuki et al. 2003). Lin et al. (2013) showed that the Itozawa and Yunodake faults, which are in similar Cretaceous granitoid and metamorphic rocks, also have layered gouge and breccia zones comparable to those we documented on the Mochiyama fault and that these faults have been active normal faults since Neogene time. These cases reinforce our observations in implying that activity on the Mochiyama fault has been persistent at shallow depths. Field surveys and observations of FFZs are still important and powerful methods for fault assessment in these inland areas where well-hidden active faults have yet to be mapped.

#### Conclusion

We conducted differential InSAR analyses and field surveys in the southern Abukuma Mountains where very similar normal-type earthquakes occurred in 2011 ( $M_w$  5.8) and 2016 ( $M_w$  5.9), triggered by postseismic crustal deformation from the 2011 Tohoku-Oki earthquake. The InSAR analyses showed that both events produced linear surface displacement and areas of deformation in the same locations, indicating the presence of an active normal fault that we have named the Mochiyama fault. The 2011 event had slightly greater displacement and a slightly larger deformation area than the 2016 event. Our field surveys conducted immediately after both events documented tectonic surface ruptures and repeated damage to artificial structures along the linear surface displacement. Slickenlines and fault orientations in FFZs are concordant with the fault models of both events. These observations indicate that the Mochiyama fault reactivated within a very short time interval and behaved with semicharacteristic slip, with similar distributions but slightly different amounts of slip. InSAR analysis is a powerful tool for characterizing

fault behavior in moderate seismic events, even in mountainous settings.

Our trench excavation and radiocarbon dating suggest that the Mochiyama fault ruptured in synchrony with the Yunodake fault in the case of the 2011 Tohoku-Oki earthquake and possibly in the case of the AD 869 Jogan megathrust earthquake, but we cannot rule out the possibility that only the Mochiyama fault ruptured in connection with the AD 869 or other megathrust events. An important possibility of this and other paleoseismic studies is that normal faults in the southern Abukuma Mountains have not been consistently synchronized with the Japan Trench megathrust supercycle of 500–700 years. The case of 2011, in which the Yunodake, Itozawa, and Mochiyama faults were all triggered, appears to be a rare occurrence.

The layered FFZs and subtle tectonic geomorphic features visible in a lidar DEM both indicate repeated faulting of the Mochiyama fault. However, the fault is invisible in aerial photographs due to dense forest and its slow slip rate, which we infer to be no greater than  $\sim 0.1$  mm/year. Detection in lidar DEMs, followed by thorough field surveys and observations of FFZs, is an important method for assessments of such slow slip rate faults.

The semicharacteristic behavior of the Mochiyama fault and the complex paleoseismic history of the Abukuma Mountains, as well as examples elsewhere, show that normal faults in the hanging wall of megathrust events respond irregularly to changes in extensional stress regardless of their magnitude. Irregular activity on inland normal faults should be expected after future megathrust earthquakes.

## Supplementary information

**Supplementary information** accompanies this paper at <https://doi.org/10.1186/s40623-019-1085-8>.

**Additional file 1: Fig. S1.** Schematic diagram showing the differences in incidence angles and resulting LOS values between PALSAR (2011 event) and PALSAR-2 (2016 and post-2016 event). Estimated difference in vertical offsets is  $\sim 2.7\%$ , which is considered negligible. **Fig. S2.** Geologic map of the study area adapted from Kubo et al. (2007); location in Fig. 1. Also shown are small notches and wind gaps on ridge crests as well as fluvial terraces, identified in aerial photographs and a lidar DEM. **Fig. S3.** MPI-RRIM maps (locations in Fig. 2a) based on 2-m lidar DEMs. Location of 2016 surface ruptures and minor cracks, FFZs, subtle small notches, and wind gaps on ridge crests are shown. **Fig. S4.** Photographs of **a** the Mochiyama trench excavation, **b** the Koyama Dam FFZ, and **c** the Wakaguri FFZ, fresh slickenlines in gouge of **d** the Mochiyama trench and **e** the Koyama Dam FFZ, **f** displaced clay fragments within gouge of the Koyama Dam FFZ, and **g** subtle slickenlines in gouge of the Wakaguri FFZ. **Fig. S5.** Photomosaics of the **a** east wall and **b** west wall of the Mochiyama trench with fiducial grid overlay. Sketch log of this trench is shown in Fig. 7.

**Additional file 2.** KML files showing locations of features associated with the 2011 and 2016 events. Red pins indicate tectonic surface ruptures, green pins indicate other minor cracks, and yellow stars indicate the locations of FFZs.

## Abbreviations

InSAR: interferometric synthetic aperture radar; DEM: digital elevation model; FFZ: fault fracture zone; GNSS: global navigation satellite system; LOS: line of sight; PALSAR: phased array-type L-band synthetic aperture radar; ALOS: advanced land observing satellite; GSI: Geospatial Information Authority of Japan; SD: surface displacement; FD: flexure displacement; MPI-RRIMs: morphometric protection index red relief image maps.

## Acknowledgements

The lidar DEM data were provided by Yasuo Awata and Masayuki Yoshimi of the Geological Survey of Japan, AIST. Yamato Watanabe of CERES Co., Ltd. supported the 2017 field surveys. Kazuhiko Okazaki and Yusuke Komine of Dia Consultants Co., Ltd. supported and managed the trench excavations. We benefited from discussions with Masashi Omata of PASCO Co., Ltd. about post-seismic deformation detected by InSAR analysis and with Akiko Miyawaki of Hanshin Consultants Co., Ltd. about tectonic geomorphology. Takumi Onuma of JGI, Inc. provided InSAR data for the 2011 earthquake and useful advice for InSAR analyses. Toshinori Sasaki of CRIEPI supported the 2011 field survey, and Keiichi Ueta of CRIEPI supported our field surveys and provided useful advice on trench observations. PALSAR-2 data partially used in this study were supplied by JAXA in the framework of JAXA's Landslide Disaster Working Group and a cooperative research 2018-B-02 of ERI, Univ. of Tokyo. Analysis of the data was partially supported by KAKEN 17K0123. Helpful comments from three anonymous reviewers and the editor Dr. Takeo Ito improved our articles.

## Authors' contributions

KK conducted all fieldwork, made geomorphic observations, and drafted the manuscript. KA made observations and helped with the logging of FFZs. TN conducted field surveys and managed the trench excavations. HPS conducted the InSAR analysis and provided useful advice. AY supported logging and sampling in the trench excavations. YA provided the field data for the 2011 event and provided useful advice for InSAR analysis. All authors read and approved the final manuscript.

## Funding

This work was financially supported in part by the Central Research Institute of Electric Power Industry (CRIEPI) under its "Fault survey for recent earthquakes" program. InSAR processing was financially supported in part by KAKENHI grant 17H02973 from the Japan Society for Promotion of Science.

## Availability of data and materials

The datasets supporting the conclusions of this article are included within the article and its additional files. Correspondence and requests for materials should be addressed to KK.

## Competing interests

The authors declare that they have no competing interests.

## Author details

<sup>1</sup> Central Research Institute of Electric Power Industry, 1646 Abiko, Abiko-shi, Chiba 270-1194, Japan. <sup>2</sup> Graduate School of Science and Engineering, Chiba University, 1-33 Yayoi-cho, Inage-ku, Chiba-shi, Chiba 263-8522, Japan. <sup>3</sup> Dia Consultants Co., Ltd., 2-272-3 Yoshino-cho, Kita-ku, Saitama-shi, Saitama 331-0811, Japan. <sup>4</sup> Department of Geography, College of Humanities and Sciences, Nihon University, 3-25-40 Sakurajosui, Setagaya-ku, Tokyo 156-8550, Japan. <sup>5</sup> CERES Co., Ltd., 1646 Abiko, Abiko-shi, Chiba 270-1194, Japan.

Received: 1 May 2019 Accepted: 2 October 2019

Published online: 18 October 2019

## References

- Aiyama K, Tanaka S, Sasaki T (2017) Consideration of the activity of a fault based on detailed structural analysis of a fault fracture zone. *J Japan Soc Eng Geol Japan Soc Eng Geol* 58:2–18. <https://doi.org/10.5110/jjseg.58.2> (in Japanese with English abstract)
- Argus DF, Gordon RG, Demets C (2011) Geologically current motion of 56 plates relative to the no-net-rotation reference frame. *Geochem Geophys Geosystems* 12:Q11001. <https://doi.org/10.1029/2011GC003751>

- Biasi GP, Weldon R (1994) Quantitative refinement of calibrated  $^{14}\text{C}$  distributions. *Quat Res* 41:1–18. <https://doi.org/10.1006/qres.1994.1001>
- Bronk Ramsey C (2017) Methods for summarizing radiocarbon datasets. *Radiocarbon* 59:1809–1833. <https://doi.org/10.1017/RDC.2017.108>
- Brozzetti F, Boncio P, Cirillo D et al (2019) High-resolution field mapping and analysis of the August–October 2016 coseismic surface faulting (Central Italy earthquakes): slip distribution, parameterization, and comparison with global earthquakes. *Tectonics* 38:417–439. <https://doi.org/10.1029/2018TC005305>
- Chen CW, Zebker HA (2002) Phase unwrapping for large SAR interferograms: statistical segmentation and generalized network models. *IEEE Trans Geosci Remote Sens* 40:1709–1719. <https://doi.org/10.1109/TGRS.2002.802453>
- Choi JH, Ko K, Gihm YS et al (2019) Surface deformations and rupture processes associated with the 2017  $M_w$  5.4 Pohang, Korea, earthquake. *Bull Seismol Soc Am* 109:756–769. <https://doi.org/10.1785/0120180167>
- Civico R, Pucci S, De Martini PM, Pantosti D (2015) Morphotectonic analysis of the long-term surface expression of the 2009 L'Aquila earthquake fault (Central Italy) using airborne LiDAR data. *Tectonophysics* 644:108–121. <https://doi.org/10.1016/j.tecto.2014.12.024>
- Ferrario MF, Livio F (2018) Characterizing the distributed faulting during the 30 October 2016, Central Italy Earthquake: a reference for fault displacement hazard assessment. *Tectonics* 37:1256–1273. <https://doi.org/10.1029/2017TC004935>
- Fujiwara O, Sanga T, Ohomori H (2001) Regional distribution of erosion rates over the Japanese Islands (CD-ROM version). Japan Nuclear Cycle Development Institute Technical Report 41, 25p.+ CD-ROM **(in Japanese with English abstract)**
- Fujiwara S, Yurai H, Kobayashi T et al (2016) Small-displacement linear surface ruptures of the 2016 Kumamoto earthquake sequence detected by ALOS-2 SAR interferometry. *Earth Planets Space* 68:160. <https://doi.org/10.1186/s40623-016-0534-x>
- Fujiwara S, Nakano T, Morishita Y et al (2019) Detection and interpretation of local surface deformation from the 2018 Hokkaido Eastern Iburu Earthquake using ALOS-2 SAR data. *Earth Planets Space* 71:64. <https://doi.org/10.1186/s40623-019-1046-2>
- Fukushima Y, Takada Y, Hashimoto M (2013) Complex ruptures of the 11 April 2011  $M_w$  6.6 Iwaki earthquake triggered by the 11 March 2011  $M_w$  9.0 Tohoku earthquake, Japan. *Bull Seismol Soc Am* 103:1572–1583. <https://doi.org/10.1785/0120120140>
- Fukushima Y, Toda S, Miura S et al (2018) Extremely early recurrence of intraplate fault rupture following the Tohoku-Oki earthquake. *Nat Geosci* 11:777–781. <https://doi.org/10.1038/s41561-018-0201-x>
- Goldstein RM, Werner CL (1998) Radar interferogram filtering for geophysical applications. *Geophys Res Lett* 25:4035–4038. <https://doi.org/10.1029/1998GL900033>
- Imaizumi T, Miyauchi T, Tsutsumi H et al (eds) (2018) Digital active fault map of Japan. University of Tokyo Press, Tokyo **(in Japanese)**
- Imanishi K, Ando R, Kuwahara Y (2012) Unusual shallow normal-faulting earthquake sequence in compressional northeast Japan activated after the 2011 off the Pacific coast of Tohoku earthquake. *Geophys Res Lett* 39:L09306. <https://doi.org/10.1029/2012GL051491>
- Ishimura D, Toda S, Mukoyama S et al (2019) 3D Surface displacement and surface ruptures associated with the 2014  $M_w$  6.2 Nagano earthquake using differential lidar. *Bull Seismol Soc Am*. <https://doi.org/10.1785/0120180020>
- Kaneda H (2003) Threshold of geomorphic detectability estimated from geologic observations of active low slip-rate strike-slip faults. *Geophys Res Lett* 30:1238. <https://doi.org/10.1029/2002GL016280>
- Kaneda H, Chiba T (2019) Stereopaired morphometric protection index red relief image maps (Stereo MPI-RRIMs): effective visualization of high-resolution digital elevation models for interpreting and mapping small tectonic geomorphic features. *Bull Seismol Soc Am* 109:99–109. <https://doi.org/10.1785/0120180166>
- Kaneda H, Okada A (2008) Long-term seismic behavior of a fault involved in a multiple-fault rupture: insights from tectonic geomorphology along the Neodani Fault, central Japan. *Bull Seismol Soc Am* 98:2170–2190. <https://doi.org/10.1785/0120070204>
- Kato A, Sakai S, Obara K (2011) A normal-faulting seismic sequence triggered by the 2011 off the Pacific coast of Tohoku earthquake: wholesale stress regime changes in the upper plate. *Earth Planets Space* 63:745–748. <https://doi.org/10.5047/eps.2011.06.014>
- Kobayashi T, Tobita M, Nishimura T et al (2011) Crustal deformation map for the 2011 off the Pacific coast of Tohoku earthquake, detected by InSAR analysis combined with GEONET data. *Earth Planets Space* 63:621–625. <https://doi.org/10.5047/eps.2011.06.043>
- Kubo K, Yanagisawa Y, Yamamoto T, et al. (2007) Geological map of Japan 1:200,000, Shirakawa. Geol Soc Jpn AIST **(in Japanese)**
- Lin A, Toda S, Rao G et al (2013) Structural analysis of coseismic normal fault zones of the 2011  $M_w$  6.6 Fukushima earthquake, northeast Japan. *Bull Seismol Soc Am* 103:1603–1613. <https://doi.org/10.1785/0120120111>
- Livio F, Kettermann M, Reicherter K, Urai JL (2019) Growth of bending-moment faults due to progressive folding: insights from sandbox models and paleoseismological implications. *Geomorphology* 326:152–166. <https://doi.org/10.1016/j.geomorph.2018.02.012>
- McCalpin JP (2009) Chapter 9 Application of paleoseismic data to seismic hazard assessment and neotectonic research. *Int Geophys* 62:439–493. [https://doi.org/10.1016/s0074-6142\(96\)80076-3](https://doi.org/10.1016/s0074-6142(96)80076-3)
- Meneses-Gutierrez A, Sagiya T (2016) Persistent inelastic deformation in central Japan revealed by GPS observation before and after the Tohoku-oki earthquake. *Earth Planet Sci Lett* 450:366–371. <https://doi.org/10.1016/j.epsl.2016.06.055>
- Milliner CWD, Dolan JF, Hollingsworth J et al (2015) Quantifying near-field and off-fault deformation patterns of the 1992  $M_w$  7.3 Landers earthquake. *Geochem Geophys Geosystems* 16:1577–1598. <https://doi.org/10.1002/2014GC005693>
- Miyashita Y (2018) Holocene paleoseismic history of the Yunodake fault ruptured by the 2011 Fukushima-ken Hamadori earthquake, Fukushima Prefecture, Japan. *Geomorphology* 323:70–79. <https://doi.org/10.1016/j.geomorph.2018.08.040>
- Mizoguchi K, Uehara SI, Ueta K (2012) Surface fault ruptures and slip distributions of the  $M_w$  6.6 11 April 2011 Hamadori, Fukushima prefecture, Northeast Japan, earthquake. *Bull Seismol Soc Am* 102:1949–1956. <https://doi.org/10.1785/0120110308>
- Nakamura A, Yokoyama Y, Shiroya K et al (2014) Direct comparison of site-specific and basin-scale denudation rate estimation by in situ cosmogenic nuclides: an example from the Abukuma Mountains, Japan. *Prog Earth Planet Sci* 1:9. <https://doi.org/10.1186/2197-4284-1-9>
- Namegaya Y, Satake K (2014) Reexamination of the A.D. 869 Jogan earthquake size from tsunami deposit distribution, simulated flow depth, and velocity. *Geophys Res Lett* 41:2297–2303. <https://doi.org/10.1002/2013GL058678>
- Niwa Y, Toda S, Omata M et al (2013) Paleoseismic events of the Itozawa fault prior to the 2011 Fukushima-ken-hamadori earthquake revealed from a borehole survey at Shionohira, Iwaki City, Fukushima Prefecture, Japan. *Acta Fault Res* 2013:1–7. [https://doi.org/10.11462/af.2013.39\\_1](https://doi.org/10.11462/af.2013.39_1) **(in Japanese with English abstract)**
- Okada T, Yoshida K, Ueki S et al (2011) Shallow inland earthquakes in NE Japan possibly triggered by the 2011 off the Pacific coast of Tohoku earthquake. *Earth Planets Space* 63:749–754. <https://doi.org/10.5047/eps.2011.06.027>
- Otsubo M, Miyakawa A, Imanishi K (2018) Normal-faulting stress state associated with low differential stress in an overriding plate in northeast Japan prior to the 2011  $M_w$  9.0 Tohoku earthquake. *Earth Planets Space* 70:51. <https://doi.org/10.1186/s40623-018-0813-9>
- Otsuki K, Monzawa N, Nagase T (2003) Fluidization and melting of fault gouge during seismic slip: identification in the Nojima fault zone and implications for focal earthquake mechanisms. *J Geophys Res Solid Earth*. <https://doi.org/10.1029/2001jb001711>
- Ozawa T, Shimizu S (2010) Atmospheric noise reduction in InSAR analysis using numerical weather model. *J Geod Soc Jpn* 56:137–147. <https://doi.org/10.11366/sokuchi.56.137> **(in Japanese with English abstract)**
- Ozawa T, Fujita E, Ueda H (2016) Crustal deformation associated with the 2016 Kumamoto earthquake and its effect on the magma system of Aso volcano. *Earth Planets Space* 68:186. <https://doi.org/10.1186/s40623-016-0563-5>
- Paul D, Mitra S (2015) Fault patterns associated with extensional fault-propagation folding. *Mar Pet Geol* 67:120–143. <https://doi.org/10.1016/j.marpetgeo.2015.04.020>
- Ponti DJ, Rosa CM, and Blair JL (2019) The  $M_w$  6.0 South Napa earthquake of August 24, 2014—Observations of surface faulting and ground deformation, with recommendations for improving post-earthquake field

- investigations. U.S. Geological Survey Open-File Report 2019–1018, 50 p 15 appendixes. <https://doi.org/10.3133/ofr20191018>
- Research Group for Active Faults (1980) Active faults in Japan, sheet maps and inventories. Univ. Tokyo Press, Tokyo, pp 134–135 **(in Japanese)**
- Research Group for Active Faults (1991) Active faults in Japan, sheet maps and inventories. Univ. Tokyo Press, Tokyo, pp 162–163
- Satake K (2015) Geological and historical evidence of irregular recurrent earthquakes in Japan. *Philos Trans R Soc A Math Phys Eng Sci*. <https://doi.org/10.1098/rsta.2014.0375>
- Satake K, Fujii Y (2014) Review: source models of the 2011 Tohoku earthquake and long-term forecast of large earthquakes. *J Disaster Res* 9:272–280. <https://doi.org/10.20965/jdr.2014.p0272>
- Sato HP, Une H (2016) Detection of the 2015 Gorkha earthquake-induced landslide surface deformation in Kathmandu using InSAR images from PALSAR-2 data the 2015 Gorkha, Nepal, Earthquake and Himalayan Studies: First Results 4. *Seismology*. *Earth Planets Space* 68:47. <https://doi.org/10.1186/s40623-016-0425-1>
- Sawai Y, Namegaya Y, Okamura Y et al (2012) Challenges of anticipating the 2011 Tohoku earthquake and tsunami using coastal geology. *Geophys Res Lett*. <https://doi.org/10.1029/2012GL053692>
- Sawai Y, Namegaya Y, Tamura T et al (2015) Shorter intervals between great earthquakes near Sendai: scour ponds and a sand layer attributable to A.D. 1454 overwash. *Geophys Res Lett* 42:4795–4800. <https://doi.org/10.1002/2015GL064167>
- Schwartz DP, Coppersmith KJ (1984) Fault behavior and characteristic earthquakes: examples from the Wasatch and San Andreas fault zones (USA). *J Geophys Res* 89:5681–5698. <https://doi.org/10.1029/JB089iB07p05681>
- Scott CP, Arrowsmith JR, Nissen E et al (2018) The M7 2016 Kumamoto, Japan, Earthquake: 3-D deformation along the fault and within the damage zone constrained from differential lidar topography. *J Geophys Res Solid Earth* 123:6138–6155. <https://doi.org/10.1029/2018JB015581>
- Scott CP, Champenois J, Klinger Y et al (2019) The 2016 M7 Kumamoto, Japan, earthquake slip field derived from a joint inversion of differential lidar topography, optical correlation, and InSAR surface displacements. *Geophys Res Lett*. <https://doi.org/10.1029/2019gl082202>
- Sheppard JC (1975) A radiocarbon dating primer. Bull 338. Washington State University, College of Engineering Research Pullman, WA
- Shigetomi M, Lin A (1999) Seismic events inferred from the layering structures of fault gouge zone and pseudotachylytes in the Nojima fault zone, Japan. *Struct Geol (Jour Tecton Res Gp Japan)* 43:33–42 **(in Japanese with English abstract)**
- Sibson RH (1977) Fault rocks and fault mechanisms. *J Geol Soc London* 133:191–213. <https://doi.org/10.1144/gsjgs.133.3.0191>
- Sieh K (1996) The repetition of large-earthquake ruptures. *Proc Natl Acad Sci* 93:3764–3771. <https://doi.org/10.1073/pnas.93.9.3764>
- Suwa Y, Miura S, Hasegawa A et al (2006) Interplate coupling beneath NE Japan inferred from three-dimensional displacement field. *J Geophys Res Solid Earth* 111:B04402. <https://doi.org/10.1029/2004JB003203>
- Takagi H, Kobayashi K (1996) Dynamic evolution of deformation microstructures in rocks. Kinematics, particularly the estimation of non-coaxiality in deformed rocks. Composite planar fabrics of fault gouges and mylonites-comparative petrofabrics. *J Geol Soc Japan* 102:170–179. <https://doi.org/10.5575/geosoc.102.170> **(in Japanese with English abstract)**
- Toda S, Tsutsumi H (2013) Simultaneous reactivation of two, subparallel, inland normal faults during the  $M_w$  6.6 11 April 2011 Iwaki earthquake triggered by the  $M_w$  9.0 Tohoku-oki, Japan, earthquake. *Bull Seismol Soc Am* 103:1584–1602. <https://doi.org/10.1785/0120120281>
- Toda S, Stein RS, Lin J (2011) Widespread seismicity excitation throughout central Japan following the 2011  $M=9.0$  Tohoku earthquake and its interpretation by Coulomb stress transfer. *Geophys Res Lett* 38:7. <https://doi.org/10.1029/2011gl047834>
- Usami T (2013) Materials for comprehensive list of destructive earthquakes in Japan, 599–2012, revised in 2013. Univ Tokyo Press Tokyo **(in Japanese)**
- Usami K, Ikehara K, Kanamatsu T, McHugh CM (2018) Super-cycle in great earthquake recurrence along the Japan Trench over the last 4000 years. *Geosci Lett* 5:11. <https://doi.org/10.1186/s40562-018-0110-2>
- Villani F, Civico R, Pucci S et al (2018) A database of the coseismic effects following the 30 October 2016 Norcia earthquake in Central Italy. *Sci Data* 5:180049. <https://doi.org/10.1038/sdata.2018.49>
- Wei M, Sandwell D, Fialko Y, Bilham R (2011) Slip on faults in the Imperial Valley triggered by the 4 April 2010  $M_w$  7.2 El Mayor-Cucapah earthquake revealed by InSAR. *Geophys Res Lett* 38:01308. <https://doi.org/10.1029/2010gl045235>
- Yoshimi M (2014) Archiving fundamental data for active tectonics of east Japan: collecting high-resolution topography data in/around Tokyo Metropolitan area and digitizing orientation data in Tohoku area. *GSI Interim report* 66:229–238 **(in Japanese with English abstract)**

## Publisher's Note

Springer Nature remains neutral with regard to jurisdictional claims in published maps and institutional affiliations.

Submit your manuscript to a SpringerOpen® journal and benefit from:

- Convenient online submission
- Rigorous peer review
- Open access: articles freely available online
- High visibility within the field
- Retaining the copyright to your article

Submit your next manuscript at ► [springeropen.com](https://www.springeropen.com)